NASA/TM–2003-211186

Scale Model Experiments on Sound Propagation From a Mach 2.5 Cold Nitrogen Jet Flowing Through a Rigid-Walled Duct With a J-Deflector

Max Kandula
Sierra Lobo, Inc. (USTDC)
John F. Kennedy Space Center, Florida 32815

Bruce Vu
YA-C2-T
John F. Kennedy Space Center, Florida 32815

April 2003

The NASA STI Program Office. . . in Profile

Since its founding, NASA has been dedicated to the advancement of aeronautics and space science. The NASA Scientific and Technical Information (STI) Program Office plays a key part in helping NASA maintain this important role.

The NASA STI Program Office is operated by Langley Research Center, the Lead Center for NASA's scientific and technical information. The NASA STI Program Office provides access to the NASA STI Database, the largest collection of aeronautical and space science STI in the world. The Program Office is also NASA's institutional mechanism for disseminating the results of its research and development activities. These results are published by NASA in the NASA STI Report Series, which includes the following report types:

- TECHNICAL PUBLICATION. Reports of completed research or a major significant phase of research that present the results of NASA programs and include extensive data or theoretical analysis. Includes compilations of significant scientific and technical data and information deemed to be of continuing reference value. NASA's counterpart of peer-reviewed formal professional papers but has less stringent limitations on manuscript length and extent of graphic presentations.

- TECHNICAL MEMORANDUM. Scientific and technical findings that are preliminary or of specialized interest, e.g., quick release reports, working papers, and bibliographies that contain minimal annotation. Does not contain extensive analysis.

- CONTRACTOR REPORT. Scientific and technical findings by NASA-sponsored contractors and grantees.

- CONFERENCE PUBLICATION. Collected papers from scientific and technical conferences, symposia, seminars, or other meetings sponsored or cosponsored by NASA.

- SPECIAL PUBLICATION. Scientific, technical, or historical information from NASA programs, projects, and missions, often concerned with subjects having substantial public interest.

- TECHNICAL TRANSLATION. English-language translations of foreign scientific and technical material pertinent to NASA's mission.

Specialized services that complement the STI Program Office's diverse offerings include creating custom thesauri, building customized data bases, organizing and publishing research results ... even providing videos.

For more information about the NASA STI Program Office, see the following:

- Access the NASA STI Program Home Page at ***http:www.sti.nasa.gov***

- E-Mail your question via the Internet to help@sti.nasa.gov

- Fax your question to the NASA STI Help Desk at (301) 621-0134

- Telephone the NASA STI Help Desk at (301) 621-0390

- Write to:
  NASA STI Help Desk
  NASA Center for AeroSpace Information
  7121 Standard Drive
  Hanover, MD 21076-1320

NASA/TM–2003-211186

Scale Model Experiments on Sound Propagation From a Mach 2.5 Cold Nitrogen Jet Flowing Through a Rigid-Walled Duct With a J-Deflector

Max Kandula
Sierra Lobo, Inc. (USTDC)
John F. Kennedy Space Center, Florida 32815

Bruce Vu
YA-C2-T
John F. Kennedy Space Center, Florida 32815

National Aeronautics and Space Administration
John F. Kennedy Space Center, Kennedy Space Center, Florida 32899-0001

April 2003

ACKNOWLEDGEMENT

The authors wish to thank several individuals for carrying out the experiments. Wayne Crawford provided assistance in conducting the test operations, including flow and pressure control, microphone setup, data acquisition, and test hardware design and fabrication. Geoffrey Rowe offered support with regard to the LabView software for high-speed data acquisition and quick-look plots. Jeff Crisafulli assisted the testing with regard to microphone calibration, instrumentation, and data acquisition. Charles Baker contributed to the testing in pneumatics area. Thanks are also due to Dr. Ravi Margasahayam of Dynacs Inc., and Danielle Ford of Embry Riddle University (and a NASA co-op) for their support in the test program. This work is supported by funding from Air Force Research Laboratory, Wright Patterson Air Force Base, Ohio, with Gregory Moster as the Technical Monitor.

Available from:

NASA Center for AeroSpace Information
7121 Standard Drive
Hanover, MD 21076-1320
(301) 621-0390

National Technical Information Service
5285 Port Royal Road
Springfield, VA 22161
(703) 487-4650

ABSTRACT

The Launch Systems Testbed (LST) represents the evolution of vibroacoustics research and development work performed at NASA John F. Kennedy Space Center (KSC) over the last 15 years. The LST is located at the Launch Equipment Test Facility (LETF) in the KSC industrial complex. The LETF is operated by Sierra Lobo, Inc., as a member of University-Affiliated Technology Development Contract (USTDC) to KSC Spaceport and Engineering and Technology Directorate (YA), with ASRC Aerospace Corporation as a the prime contractor. Trajectory Simulation Mechanism (TSM) is a major component of the LST, developed specifically to simulate nonstationary acoustic loads on launch pad structures, vehicles, and payloads. TSM enhances the capabilities within LST for simulating launch environments of future vehicles. The scaled launch environments will be used to predict the full-scale launch environment via an appropriate scaling procedure.

Air Force Research Laboratory (AFRL) has tasked NASA KSC to perform a basic technology test program in support of developing a low-cost clean pad (incorporating passive mitigation techniques) for future launch vehicles. The overall goal of the program is to develop innovative launch exhaust management systems, which effectively reduce launch acoustic environment with innovative duct designs, while eliminating traditional sound suppression water systems. Passive techniques, such as nontraditional duct geometries, resonators, and diffusers, etc., will be investigated. The overall goals are to advance innovative concepts for a clean pad while developing ideas to reduce transmitted sound via investigation and modeling of jet exhaust acoustic and flow field characteristics. The series of tests outlined in this report represent baseline tests and are geared towards defining the acoustic load environment on the TSM pad for open and closed duct configurations.

This report summarizes the cold jet acoustic testing for Mach 2.5 supersonic nitrogen jet issuing from a nozzle with 1-inch exit diameter. Acoustic data, including spectral sound power and Overall Sound Pressure Level (OASPL), are obtained both for a free jet and with the jet flowing through a rigid-walled duct with a J-deflector. The relative performance of closed duct and open duct is evaluated. The results show that the closed duct is superior to the partially open duct, and results in about 3-decibel (dB) noise reduction (near the duct axis) relative to the free jet. The location of the nozzle exit plane (NEP) relative to the duct inlet plane (DIP) has a significant effect on the acoustic field. The results suggest that the location of NEP at 10 inches above the DIP results in reduced acoustic loads relative to 5 inches above the duct inlet and 1 inch into the duct inlet.

TABLE OF CONTENTS

LIST OF FIGURES

LIST OF FIGURES (cont)

ABBREVIATIONS, ACRONYMS, AND SYMBOLS

AFRL	Air Force Research Laboratory
dB	decibel
DIP	duct inlet plane
DEP	duct exit plane
FFT	Fast Fourier Transform
FRF	Flight Readiness Firing
GL	ground level
GN_2	gaseous nitrogen
Hz	hertz
KHz	kilohertz
K	kelvin
KSC	John F. Kennedy Space Center
LETF	Launch Equipment Test Facility
LST	Launch Systems Testbed
NASA	National Aeronautics and Space Administration
NEP	nozzle exit plane
OASPL	Overall Sound Pressure Level (ref. 20 μ Pa)
1/3-OBSPL	1/3-octave band sound pressure level
PR	pressure regulator
PSD	Power Spectral Densities
psi	pound per square inch
psig	pound per square inch gage
s	second
SPL	sound pressure level (ref. 20 μ Pa)
TO	Task Order
TSM	Trajectory Simulation Mechanism
YA	Spaceport Engineering and Technology
USTDC	University-Affiliated Technology Development Contract
YA-C	Testbed and Technology Branch

Nomenclature

c =sound speed, $\sqrt{\gamma g_c R_u T / W}$, ft/s

d_j = nozzle exit diameter, ft

f = frequency, Hz

g_c = gravitational constant, (lbm-ft/lbf.s^2)

M = Mach number, u_j / c

p = pressure, lbf/ft^2

Re = Jet Reynolds number, $\rho u_j d_j / \mu$

R_u = universal gas constant, lbf.ft/(lbm-mole R)

St = Strouhal number, $f d_j / u_j$

T = temperature, R

u = axial velocity, ft/s

W = molecular weight, lbm/lbm-mole

Greek Symbols

μ = dynamic viscosity, lbm.ft/s

ρ = density, lbm/ft^3

γ = isentropic exponent

Subscripts

j = jet

s = static

t = stagnation or total, or nozzle throat

SCALE MODEL EXPERIMENTS ON SOUND PROPAGATION FROM A MACH 2.5 COLD NITROGEN JET FLOWING THROUGH A RIGID-WALLED DUCT WITH A J-DEFLECTOR

1. INTRODUCTION

Acoustic loads in a launch vehicle environment represent a principal source for inducing structural vibration and may be critical to the proper functioning of vehicle components and ground support structures and equipment in the immediate vicinity of the launch pad. A knowledge of acoustic loads, including the overall sound pressure level (OASPL), sound pressure level (SPL) spectrum, and the distribution (or correlation) of surface acoustic loads, is necessary to provide the input for vibroacoustic analysis and evaluation of structural integrity. In the design of launch vehicles, it is highly desirable that data on acoustic loads (near-field and far-field noise levels) be generated both analytically and from testing of small-scale and full-scale models. Since full-scale acoustic and vibration testing is often cost prohibitive, the option of small-scale testing combined with analysis methods remains as a practical alternative.

Noise from subsonic jets is mainly due to turbulent mixing, comprising the contributions of large-scale and fine-scale structures (Lighthill 1952, 1954). The turbulent mixing noise is mainly broadband. In perfectly expanded supersonic jets (nozzle exit plane pressure equals the ambient pressure), the large-scale mixing noise manifests itself primarily as Mach wave radiation, caused by the supersonic convection of turbulent eddies with respect to the ambient fluid [Tam 1998; Kandula and Caimi 2002]. In imperfectly expanded supersonic jets, additional noise is generated on account of broadband shock noise and screech tones.

Scale models are often used in the early design stage as a means of predicting the acoustic environment associated with flight vehicles. A detailed knowledge of the mechanisms of noise generation and noise radiation by jets is essential in designing a scale model of the noise source (Morgan et. al, 1961). In order to ensure complete similarity between model and full scale similarity of flow, similarity of noise generation, and similarity of noise propagation must be ensured.

In practice, it is generally difficult to duplicate (simulate) all the characteristic parameters in the scale model. Model testing with even smaller rocket engines requires extensive safety precautions. Heated jet facilities also involve considerable complexity and cost. The use of less expensive facilities or lower gas temperatures, for example, would considerably simplify model testing (Morgan et. al, 1961). The ability to conduct a scale-model test with a substitute gas (air, nitrogen, helium, etc.) results in considerable savings (reduced costs of test facilities, test time) and advantages (Kinzie and McLaughlin 1999). A discussion of the scaling laws for jet noise, with emphasis on temperature effects, has been recently provided in Kandula and Vu 2003.

The purpose of this program effort is to develop cold jet testing capability to simulate small-scale launch environments for use in testing and evaluation of candidate launch pad ducts for future space vehicles for AFRL. Gaseous nitrogen is exclusively tested in the present investigation.

2. OVERVIEW OF AFRL TEST PROGRAM

The AFRL research project encompasses the following four separate phases.

Phase 1 involves the design, manufacture, and installation of a pressurized nitrogen chamber with an interchangeable supersonic nozzle on the TSM and an exhaust duct composed of a J-deflector and a removable cover for simulating open and closed ducts. Additionally, Phase 1 establishes a test and measurement plan for TSM operation, transducer type, locations for acoustic and flow tests, and data acquisition hardware requirements.

Phase 2 effort consists of testing and data analysis to characterize the acoustic and flow environments of traditional closed and partially open ducts with J-deflector. In the partially open duct case (or simply the open duct case), the top cover of the duct is removed, with the sides of the duct remaining. Data is collected and analyzed for three unique supersonic jet core and plume conditions – core totally within the duct, core partially inside the duct, and core completely outside the duct. It is known that the jet core length depends on jet Mach number and jet exit temperature.

Phase 3 of the program will evaluate the effectiveness of various acoustic suppression schemes relative to the baseline tests of Phase 2.

Phase 4 requires engineering assessment of Phases 2 and 3 testing in order to classify the candidate schemes for follow-on research and development.

These baseline tests are concerned with the definition of launch exhaust acoustic environment for three unique plume – conditions plume totally within the duct, plume partially inside the duct, and plume completely outside the duct. Measurements on the TSM pad at nine separate locations around the azimuth and two separate altitudes are planned. Data analysis includes presentation of data in terms of 1/3-octave band sound pressure level (1/3-OBSPL) and OASPL.

3. TEST OBJECTIVES

The main objectives of this experimental investigation, covering Phase 1 and Phase 2, are as follows:

a. Characterize the flow and acoustic environment of a free supersonic jet

b. Characterize the acoustic environment of a supersonic jet flowing through a covered duct with a J-deflector

c. Characterize the acoustic environment of a supersonic jet flowing through an open duct with a J-deflector

4. TEST FACILITY AND INSTRUMENTATION

4.1 TEST FACILITY

The TSM located at the LETF in the KSC Industrial Area served as the primary facility for conducting the AFRL test program. It is designed to simulate $x - y$ launch trajectories for non-stationary scaled acoustic load on the launch vehicle, payload, and ground support equipment. TSM features a 1/10-scaled model of the Space Shuttle launch parameters (Figure 1). Presently, only cold jet simulation capability is available. By cold jet, it is implied here that the nozzle exit temperature is colder than the ambient temperature. The TSM facility also provides the necessary instrumentation for measurement of acoustic and exhaust flow field.

4.1.1 Nitrogen Supply

A schematic of TSM and the overall test setup is provided in Figure 2. The TSM facility is outfitted with a chamber and a supersonic nozzle. The chamber is fed from pressurized gaseous nitrogen bottles (8000 psi) in conjunction with two pressure regulators in series. The pneumatic system was modified to facilitate continuous supply of nitrogen for the duration of tests.

4.1.2 Supersonic Nozzle

The convergent-divergent nozzle was designed on the basis of characteristic method and was made of stainless steel (Figure 3). The Mach 2.5 nozzle has an exit diameter of 1 inch, compared with 3 to 4 feet of nozzle exit diameter typical of large rocket engine nozzles. The chamber and nozzle conditions for the scale model test series are displayed in Table 1. The nozzle is capable of generating sound levels in excess of about 150 dB near the NEP.

4.1.3 Exhaust Duct

A scaled aluminum exhaust duct with an upstream J-deflector (30-degree inclination to the vertical) was fabricated for installation under the nozzle. Figures 4a and 4b represent the schematics of the closed and open duct configuration respectively. A photographic view of the actual jet/duct setup is displayed in Figure 4c. The cross section of the duct is 6 inch by 12 inch. The exhaust duct can be positioned at desired levels relative to the NEP. Only static tests (with a stationary nozzle) are considered in the present investigation.

Figures 5a, 5b, and 5c show the various jet/duct configurations investigated and where the distance between the NEP and the duct inlet plane was varied. The distance between the NEP and

the duct inlet plane is varied such that the jet core is mostly outside the duct, partially inside the duct, and fully inside the duct.

4.2 INSTRUMENTATION

4.2.1 Flow Measurements

The chamber conditions (pressure and temperature) are measured by a pressure gauge and thermocouple mounted on the chamber wall. The nozzle exit conditions (exit Mach number, etc.) are obtained by a pitot tube and a static pressure probe. Details of the design of the pitot tube and the static pressure probe are not included here. Knowing the total pressure and static pressure, we can compute the exit Mach number with the aid of Rayleigh's pitot tube formula (Shapiro 1953).

4.2.2 Acoustic Measurements

Acoustic field surrounding the nozzle/duct configuration was measured by an array of acoustic transducers (microphones) placed azimuthally at 22.5-degree increments (see Figure 6). Bruel & Kjaer microphones of ½-inch diameter (B& K model 4189) were used for measuring the sound pressure level. They were placed azimuthally at 80 nozzle exit diameters from the NEP, thus representative of far field condition.

4.3 DATA ACQUISITION

4.3.1 Flow Data

Time history measurements are made of chamber pressure, chamber temperature, and pitot and static pressures at the NEP. These measurements serve to indicate the time at which steady-state conditions are achieved. Generally, it takes about 60 seconds (s) for steady conditions to prevail.

4.3.2 Acoustic Data

As soon as the flow becomes steady, recording of the acoustic data begins. Pressure-time data from the microphones are processed by the data acquisition system. The data are sampled at a maximum rate of 125,000 samples/s so that sound frequencies up to 60 kilohertz (kHz) can be recorded. With the aid of LabView software and Fast Fourier Transform (FFT), the time domain data are processed in the form of narrowband spectra, 1/3-octave-band sound pressure levels, and OASPL at each location. See appendix A.

5. TEST PROCEDURE

The chamber and the nozzle are attached to a mounting plate on the TSM horizontal carriage. This carriage is placed in the "maintenance position" and retracted towards the TSM base for all static tests. For the duct testing, the exhaust duct is installed below the nozzle at the desired lev-

els corresponding to one of the following configurations: duct inlet plane (DIP) 10 inches below the NEP (jet core mostly outside the duct; Figure 5a), DIP 5 inches below the NEP (jet core partially inside the duct; Figure 5b), and NEP 1 inch below the DIP (jet core totally inside the duct, Figure 5c). Pretest calibration of all the nine microphones is carried out. The B&K calibrator is used for this purpose, with 94 dB and 114 dB at 1 kHz.

First the pressure regulator (PR-1) is opened such that the downstream pressure is about 3000 psig. Subsequently, the second pressure regulator (PR-2) control valve is operated such that the chamber pressure (indicated by the digital readout placed close to the regulator) is at the desired value of 250 pounds per square inch gage (psia) to ensure Mach 2.5 at the nozzle exit. At this time, the chamber pressure, the pitot pressure, and the static pressure at the nozzle exit begin recording. Once the steady-state chamber pressure is achieved, as indicated by the real-time display in the control room, the acoustic data begins to be recorded. The acoustics data are taken over a period of about 4 seconds.

Posttest calibration of the microphones is carried out. Quick-look plots are then generated following the test, with the aid of the LabView-based software developed for the purpose. These plots include chamber pressure history, chamber temperature history, narrow band and 1/3 octave SPL spectrum, and OASPL distribution.

6. SAFETY CONSIDERATIONS

Proper safety procedures are followed in conducting the tests. One day prior to the test, the safety office and LETF personnel are notified. On the test date, all personnel within the 100-foot radius of the TSM pad are cleared. Additionally, no tests will be performed during lightning, at the onset of thunderstorms, or high winds in the KSC Industrial Area. The testing also adheres to the procedures within TSM Operation Technical Manual.

7. TEST MATRIX

Static nozzle tests are designed to generate steady-state flow conditions similar to Flight Readiness Firing (FRF) on the Shuttle launch pad. These steady-flow conditions with a stationary nozzle serve to define the flow and acoustic field on the TSM pad for scaling and baseline characterization. Each test is designed to record about 6 seconds of acoustic data to accurately define the nozzle exhaust environment. Tests are repeated when necessary.

Table 2 presents the test and measurement matrix. The test matrix is planned on the basis of the following considerations. Two duct configurations corresponding to open or closed ducts were considered. Three vertical duct locations - jet core mostly outside the duct (lowest duct position); jet core partially inside the duct (mid-duct position), and jet core mostly inside the duct (highest duct height) – are investigated. In order to achieve these conditions, the NEP is located 10 inches and 5 inches above the DIP, and 1 inch below the DIP. Two sensor heights of 10 inches and 53 inches above the ground were employed.

Photographic views of the free jet and the jet flowing through a closed duct are presented in Figures 7a and 7b respectively.

8. RESULTS AND COMPARISONS

8.1 RESULTS

8.1.1 Pressure and Temperature History

Figures 8a through 8m display the pressure and temperature history. In particular, the pressure plots include the history of chamber pressure (P1), pitot pressure at the NEP (P2), and the static pressure at the NEP (P3). Sensor P2 is located at the center of the NEP, and P3 is located on the nozzle axis at 1 inch downstream of the NEP. The temperature plot belongs to the chamber pressure history (P3). The pressure plots suggest that steady-state flow is achieved in about 60 to 80 seconds after the flow has started. The computed Mach number at the NEP (based on the measured values of the pitot pressure and the static pressure) is close to Mach 2.5 in accordance with the design value. Once the steady state is achieved, the acoustic data are recorded.

8.1.2 Spectral Sound Power

Figures 9a through 9n show the spectral content of sound power (1/3 octave band) for all the test cases studied. Microphone 5 is not present in most of the closed duct and open duct tests since it is the path of the flow exiting the duct. The spectral content of the sound power level for the free jet (Figure 9b) suggests that the spectral distribution is symmetric, independent of the azimuthal position of the microphone. A peak frequency of about 4 kHz is noted in this case and agrees well with the estimated value based on a Strouhal number ($St = fu_j / d_j$) of 0.2. Here f denotes the frequency, u_j the nozzle exit velocity, and d_j the nozzle exit diameter. In the closed duct case (Figure 9a) with duct inlet 10 inches below the NEP, the peak frequency near $\theta = 0$ deg. (corresponding to the duct axis) is about 4 kHz, which is close to the free jet value. However, the peak frequency increases as the angle from the jet axis is increased. Differences in the spectrum for various angles are observed over a wide range of frequencies (roughly 1.5 decades).

Figure 9i presents the spectral distribution of sound power level for the open duct configuration, with the duct inlet 10 inches below the NEP. Notable differences in the spectral behavior are observed between the closed duct and the partially open duct case. In the case of the partially open duct, significant directivity effects persist even at much lower frequencies.

8.1.3 Directivity of Overall Sound Pressure Level

The directivity of OASPL for various test runs is presented in Figures 10a through 10n. In these plots, the data for free jet (with sensors at 54 inches above ground level) are also included as a reference case. A direct comparison of the OASPL for the various jet/duct configurations is presented in the next section.

8.2 COMPARISONS

8.2.1 Effect of Ground Level

Ground effect on the OASPL is examined in Figures 11a, 11b, and 11c for the case of free jet, closed duct, and open duct respectively. In all these cases, the NEP is situated at 10 inches above the duct inlet plane. For a free jet, the ground effect at 10 inches is about 2 dB higher than that at 54 inches. The ground effect is on the order of 3 dB for the closed duct case and is the highest in the case of open duct where a ground effect of the order of about 10 dB is observed.

8.2.2 Effect of Nozzle Height Relative to the Duct Inlet Plane

Figure 12a shows a comparison of the OASPL for free jet with that of a jet passing through a closed duct, with the NEP located at different heights relative to the duct inlet. While there is axial symmetry of the OASPL for the free jet, there is considerable directivity of the OASPL in the presence of an exhaust duct. For the NEP to duct inlet distances of 5 inches and -1 inch (NEP inside the duct), the OASPL near the duct axis exceeds the value for the free jet case. When the NEP is held at 10 inches above the duct inlet, a reduction in OASPL of about 3 dB is achieved relative to the free jet case. These findings suggest that there is an optimum location of the NEP relative to the duct inlet plane, which results in the largest reduction in the OASPL [Kandula et al. 2003].

In the case of open ducts (Figure 12b), trends are contrary to the closed duct case with regard to the OAPSL variation with the duct inlet to NEP distance. For the open duct, the OASPL increases as the distance between the NEP and the duct inlet plane increases. In general, the OASPL near the duct axis for open ducts are considerably higher than that for the free jet case. This result suggests that closed ducts are preferable to open ducts as far as sound mitigation is concerned.

8.2.3 Comparison of Performance for Closed and Open Ducts

A direct comparison of the directivity of OASPL between the closed duct and the open duct is illustrated in Figures 13a through 13c for the various distances between the NEP and the duct inlet plane. As indicated earlier, for both the duct configurations when the NEP is located at 5 inches above and 1 inch below the duct inlet plane, the OASPL near the duct axis (0 to 20 degrees) exceeds that for the free jet. Only when the NEP is located at 10 inches above the duct inlet plane, it is noticed that the closed duct provides a reduction of about 3 dB (relative to the free jet) near the duct axis. In all cases, the open duct produces OASPL near the duct axis that exceeds the free jet value. As the distance between the NEP and the duct inlet plane is decreased, the deviation of OASPL for the closed duct and the open duct diminishes.

9. CONCLUSIONS

Both the closed duct and the open duct introduce considerable directivity effects. With the use of a closed duct, the overall sound power of a Mach 2.5 supersonic jet is reduced by about 3 dB near the duct axis, with higher reductions away from the duct axis. The peak frequency is found to increase above the free jet value as the angle from the jet axis is increased. The results also suggest that there is an optimum distance between the nozzle exit plane and the duct inlet for minimizing the sound power. The partially open duct results in increased sound levels near the duct axis relative to the free jet case. With regard to the closed duct, larger reductions in sound power may be realized by increasing the duct length, increasing duct cross section (adding a diffuser), and incorporating acoustic liners or resonators on the duct walls.

10. REFERENCES

Kandula, M. and Caimi, R., Simulation of jet noise with OVERFLOW CFD code and Kirchhoff surface integral, AIAA-2002-2602, 8th AIAA/CEAS Aeroacoustics Conference, June 2002.

Kandula, M. and Vu, B., On the scaling laws for jet noise in subsonic and supersonic flow, AIAA-2003-3288, 9h AIAA/CEAS Conference, Hilton Head, South Carolina, May 2003.

Kandula, M., Margasahayam, R., and Vu, B., Sound propagation from a supersonic jet flowing through a rigid-walled duct with a J-deflector, Tenth International Congress on Sound and Vibration, Stockholm, Sweden, July 7-10, 2003.

Kinzie, K.W. and McLaughlin, D.K., Measurements of supersonic helium/air mixture jets, AIAA Journal, Vol. 37, No. 11, pp. 1363-15369, 1999.

Lighthill, M.J., On Sound Generated Aerodynamically: I. General Theory, Proc. Roy. Soc. (London), Ser. A, Vol. 211, No. 1107, pp. 564-587, March 1952.

Lighthill, M.J., On Sound Generated Aerodynamically: II. Turbulence as a Source of Sound, Proc. Roy. Soc. (London), Ser. A, Vol. 222, No. 1148, pp. 1-32, Feb. 1954.

Morgan, W.V., Sutherland, L.C., and Young, K.J., The use of acoustic scale models for investigating near field noise of jet and rocket engines, WADD Technical Report 61-178, Wright Patterson Air Force Base, Ohio, 1961.

Shapiro, A., The Dynamics and Thermodynamics of Compressible Fluid Flow, Vol. 1, John Wiley, New York 1953.

Tam, C.K.W., Jet noise; since 1952, Theoretical and Computational Fluid Dynamics, Vol. 10, pp. 393-405, 1998.

Table 1. Typical Nozzle Conditions

Item	Value
Stagnation pressure, psia	251
Stagnation temperature, R	500
Nozzle exit diameter, in	1.0
Exit pressure, psia	14.7
Exit temperature, R	222
Exit velocity, ft/s	1820
Acoustic velocity at exit, ft/s	728
Nozzle exit Mach number	2.5
Exit jet Reynolds number	$4x10^6$
Ambient pressure, psia	14.7
Ambient temperature, R	540

Table 2. Summary of Mach 2.5 cold nitrogen jet acoustic test runs

Run No.	Date	Configuration	Nozzle Height (in.)*	Sensor Level (in.)	Test Duration(s)
1	11-5-02	Closed duct	10	54	70
2	11-5-02	Free jet	-	54	80
3	11-5-02	Free jet	-	10	90
4	11-5-02	Closed duct	10	10	50
5	11-7-02	Closed duct	5	54	-
6	11-7-02	Closed duct	5	10	270
7	11-7-02	Closed duct	-1	10	100
8	11-7-02	Closed duct	-1	54	P1 not steady
9	11-7-02	Closed duct	-1	54	60
10	11-13-02	Open duct	10	54	60
11	11-13-02	Open duct	10	10	70
12	11-13-02	Open duct	5	10	75
13	11-13-02	Open duct	5	54	110
14	11-21-02	Open duct	-1	54	85
15	12-11-02	Open duct	-1	54	88

Notes

*Relative to the duct inlet plane
**Relative to the ground

P1= chamber pressure.
Nozzle exit plane is 73 inches above ground.
Sensors arc radius equals 80 inches.

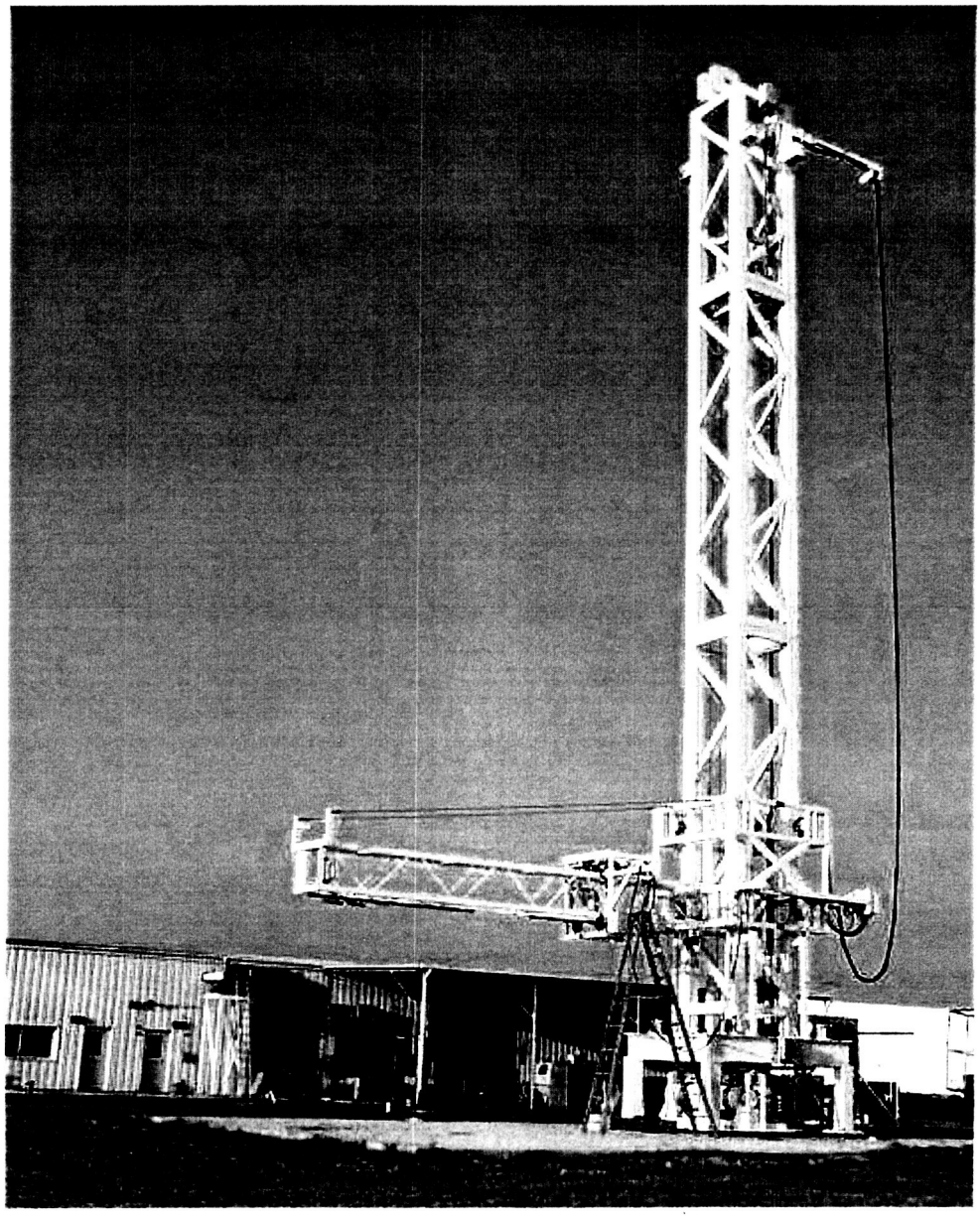

Figure 1. Trajectory simulation mechanism

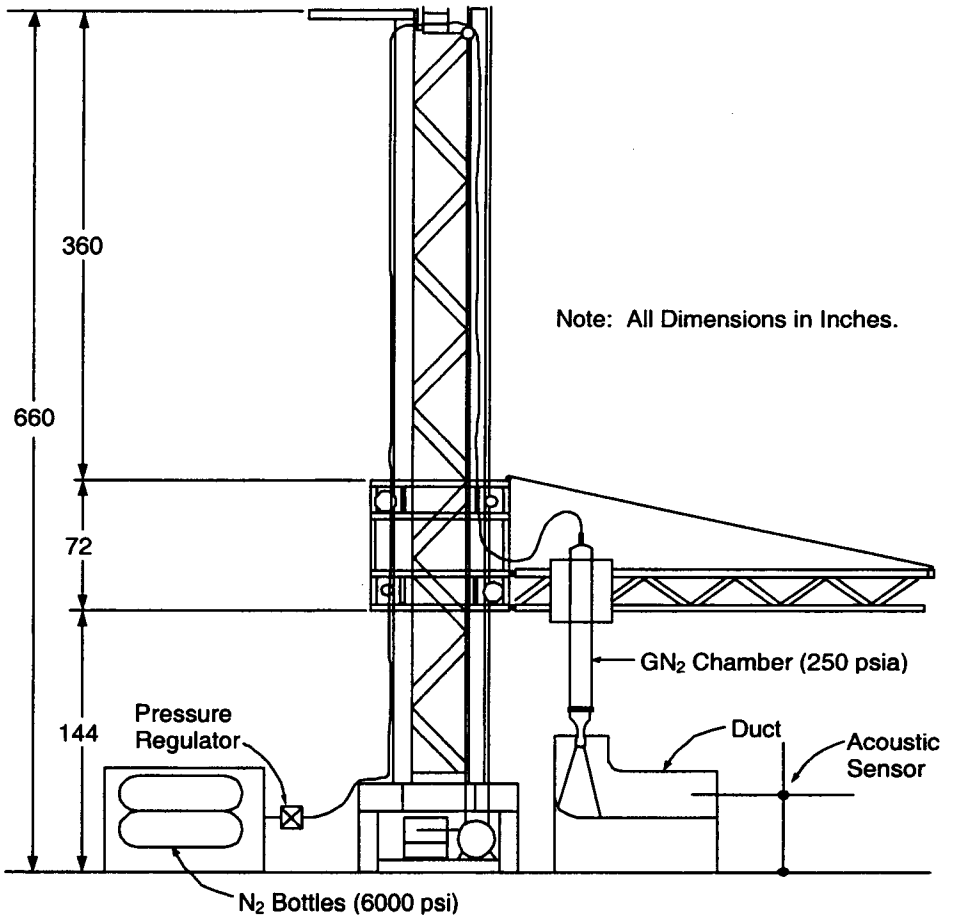

Figure 2. Overall test setup

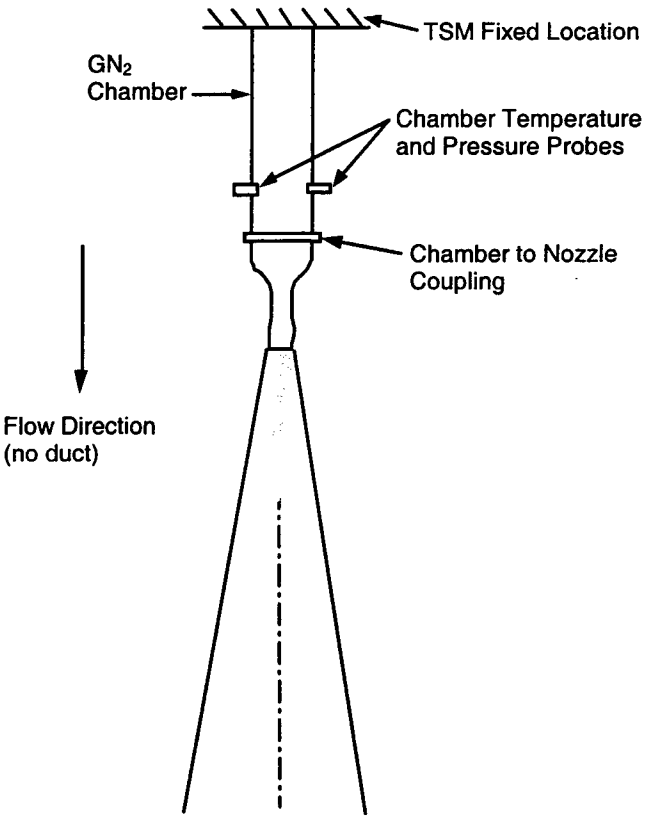

Figure 3. Free jet configuration

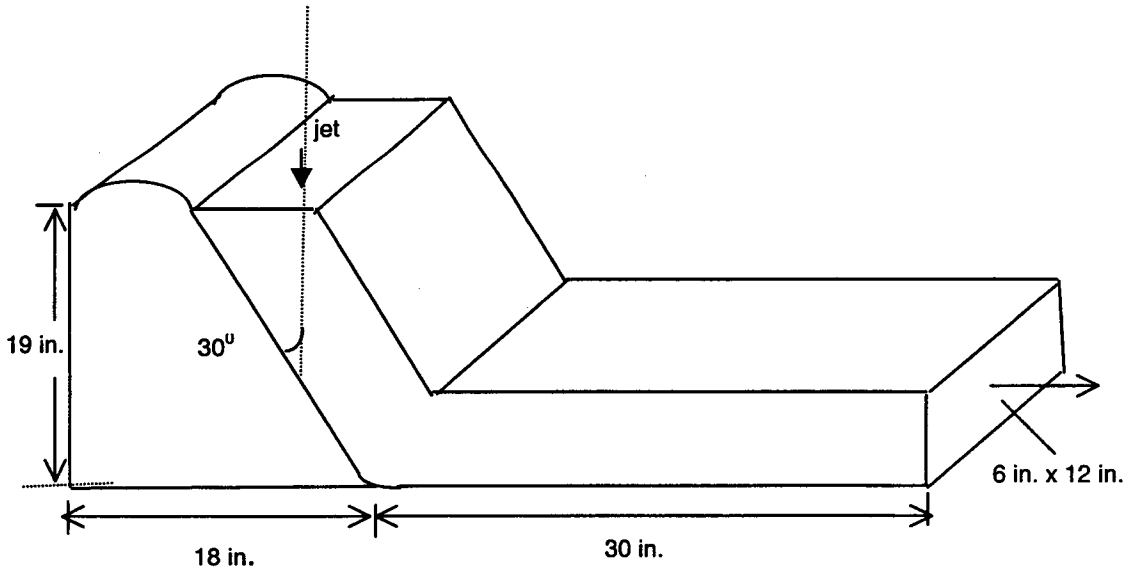

Figure. 4a. Schematic of the closed duct configuration

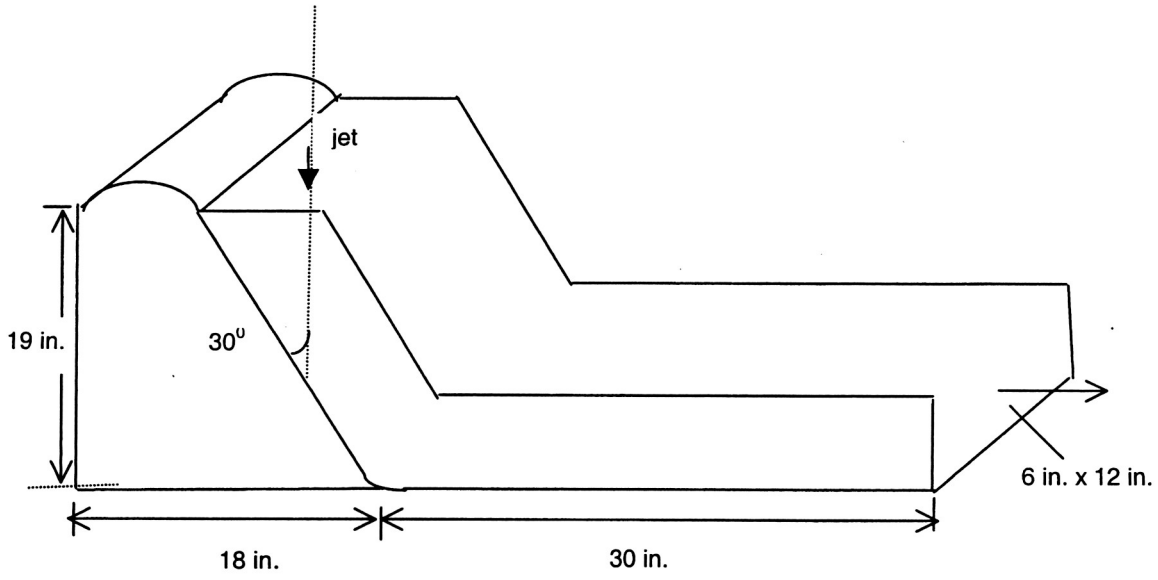

Figure 4b. Schematic of the open duct configuration

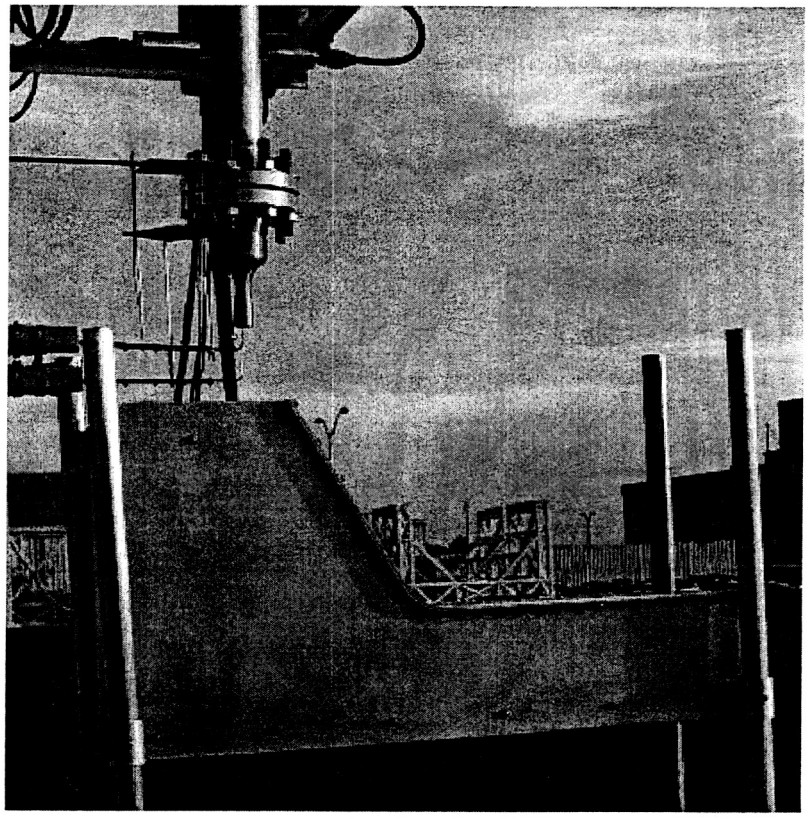

Figure 4c. Photograph of the jet/duct configuration

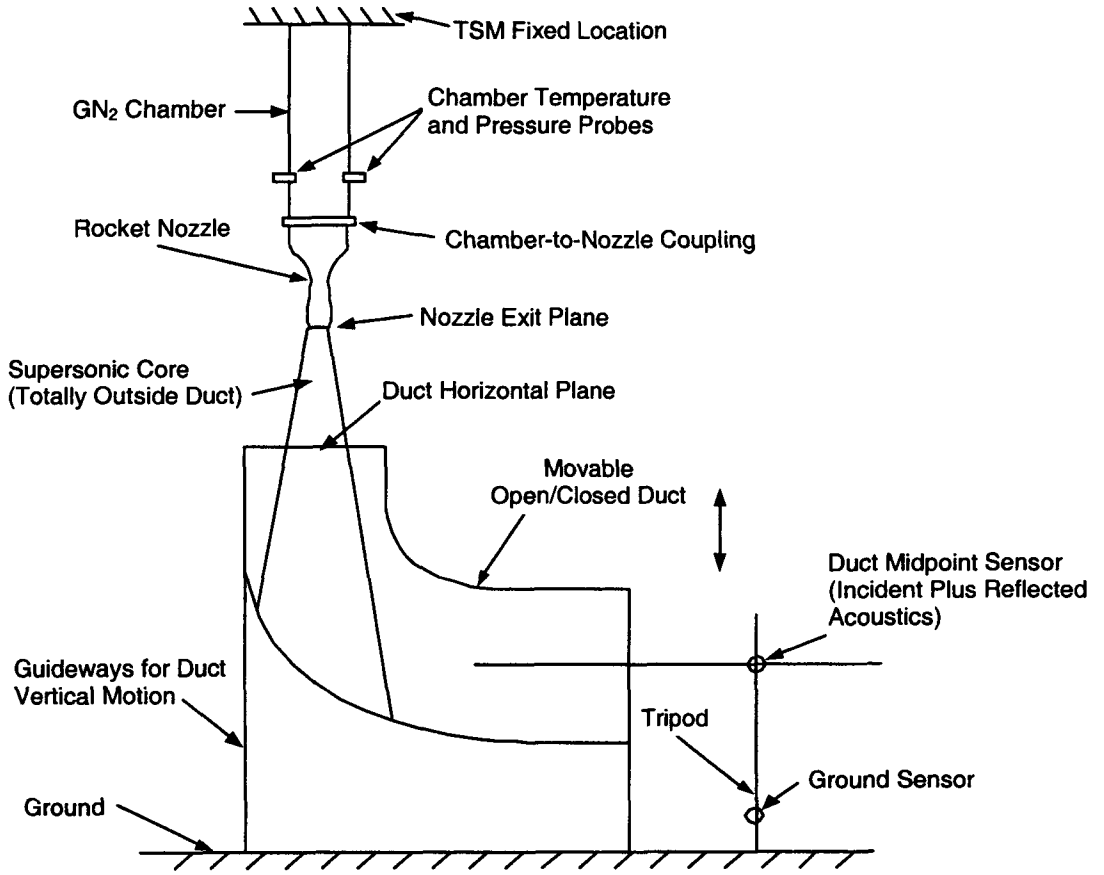

Figure 5a. Jet/duct configuration with jet core mostly outside the duct

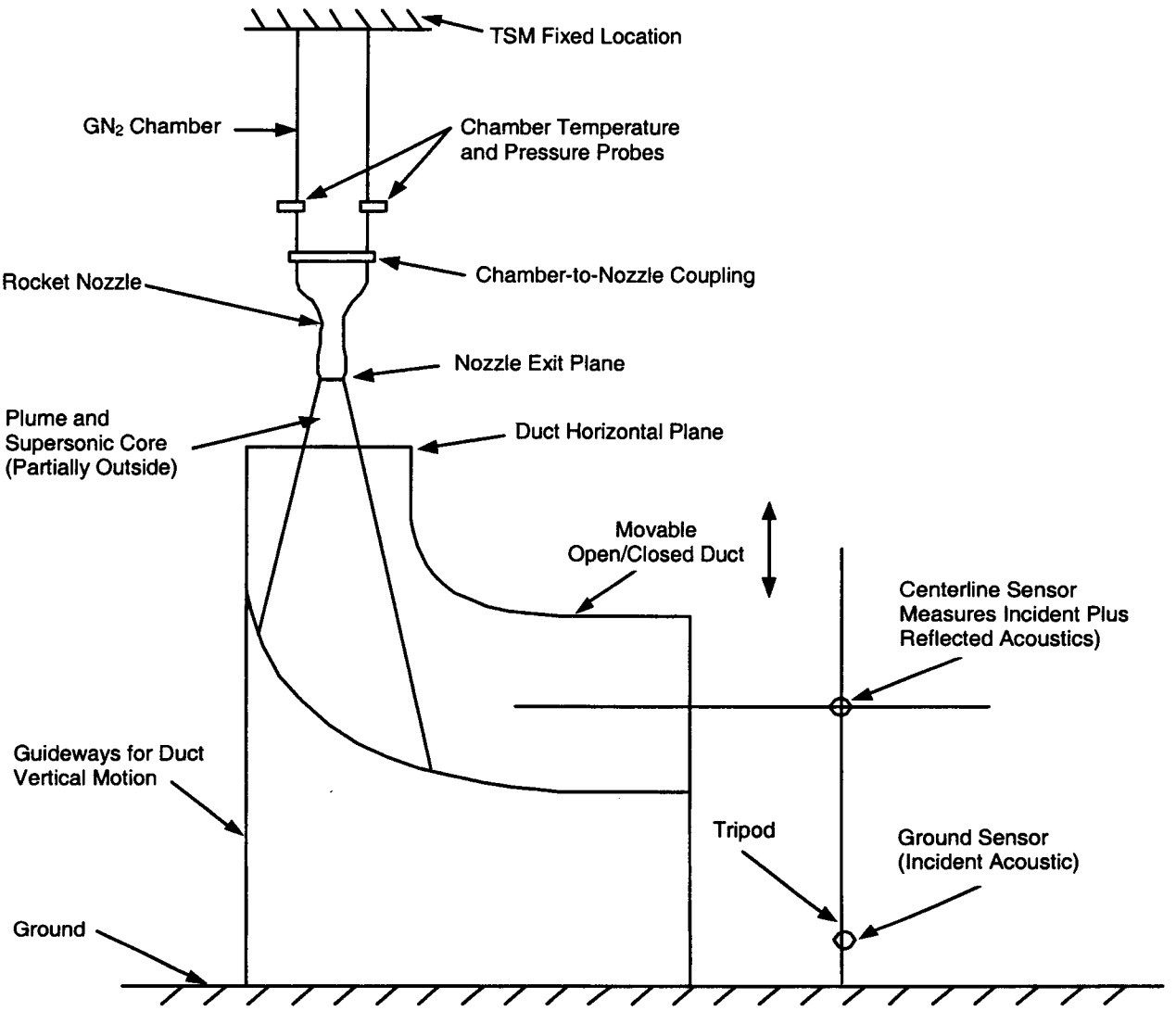

Figure 5b. Jet/duct configuration with jet core partially inside the duct

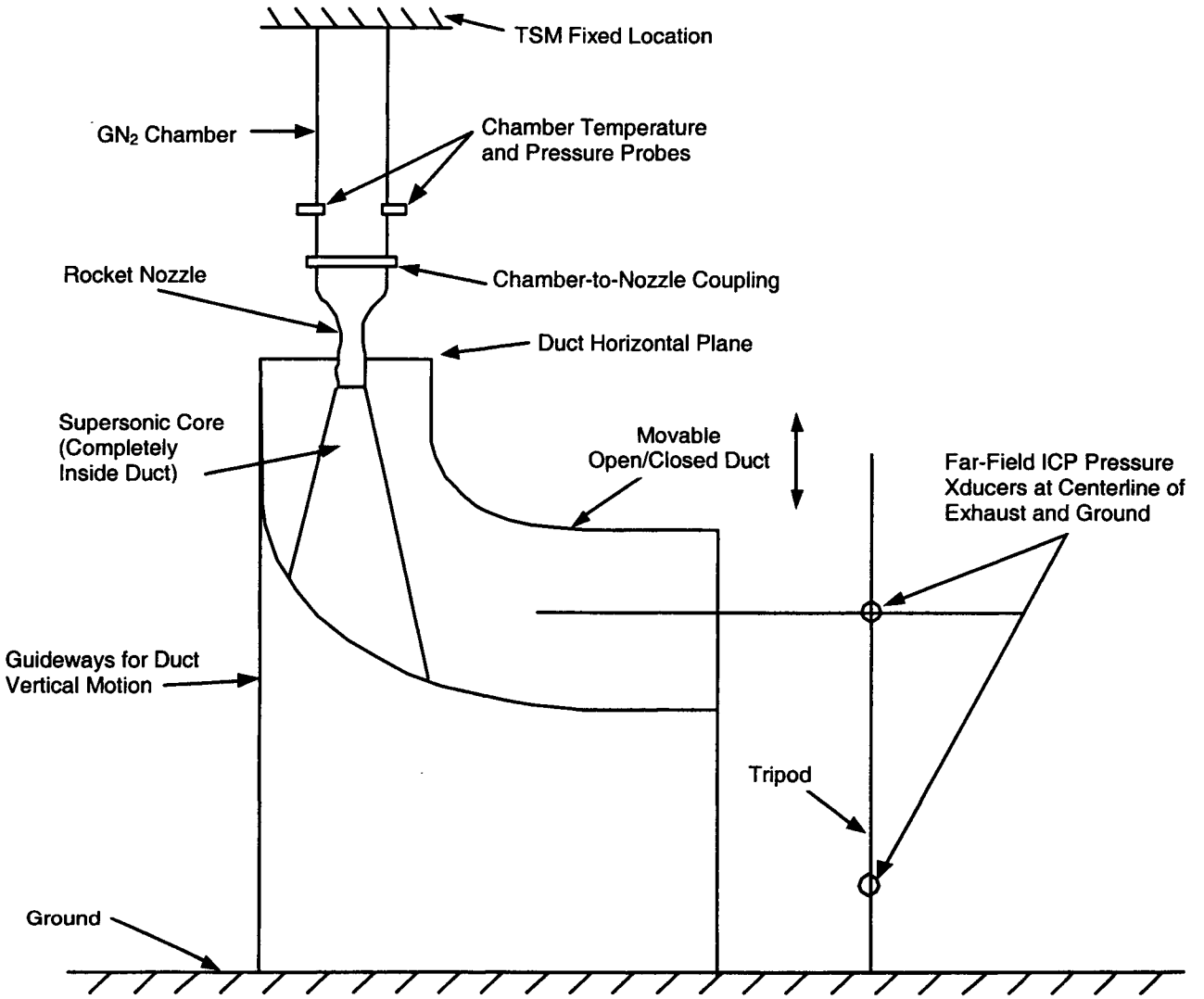

Figure 5c. Jet/duct configuration with jet core totally inside the duct

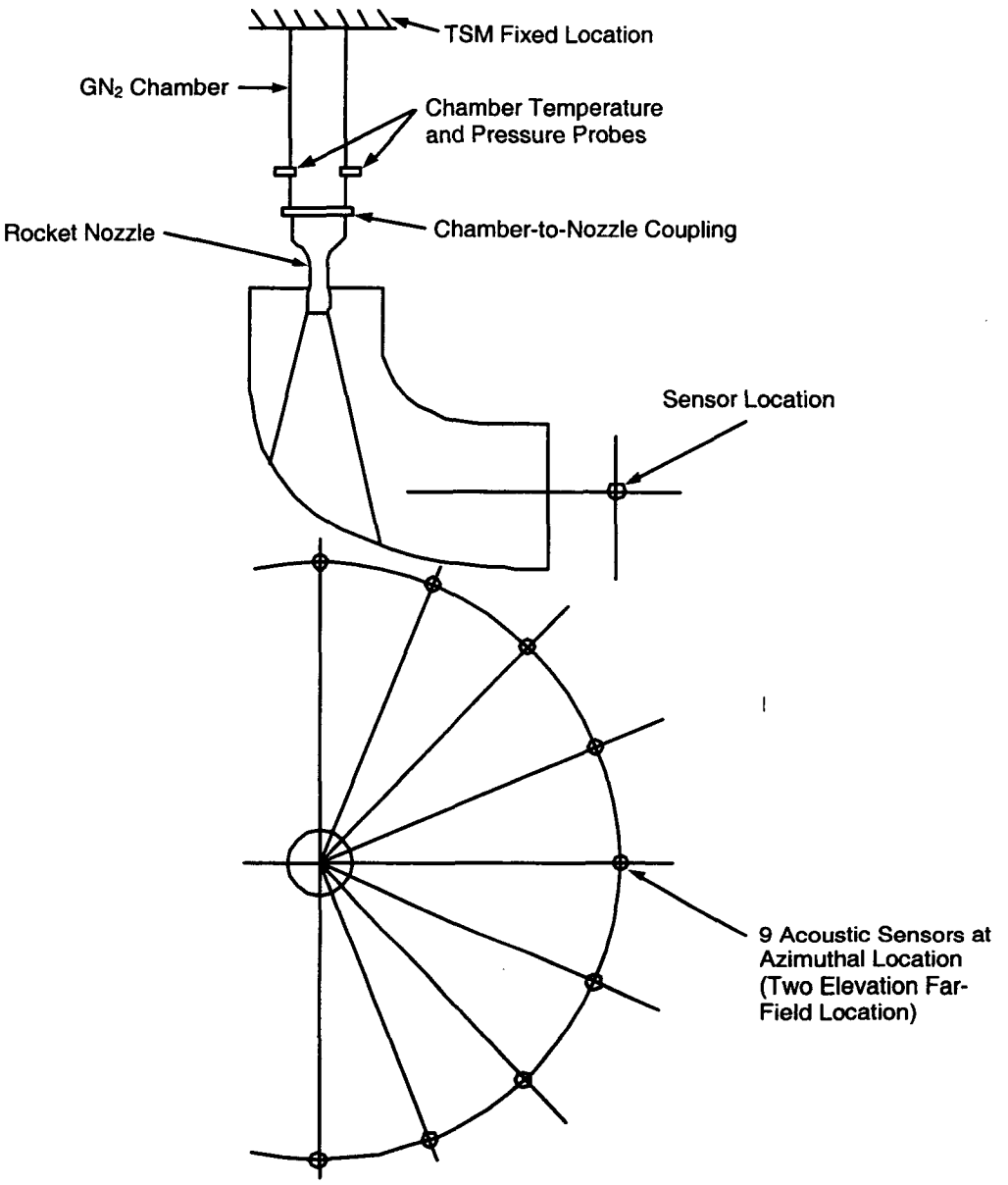

Figure 6. Microphone locations

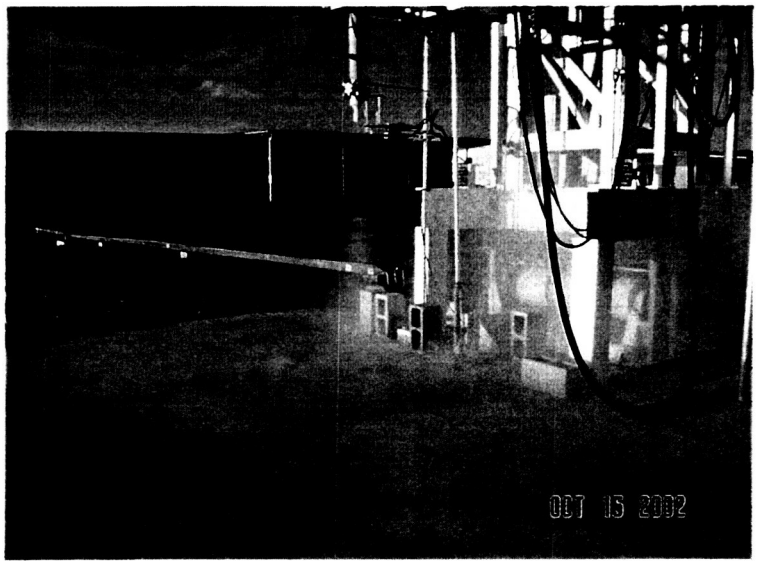

Figure 7a. Photograph of the free jet flow

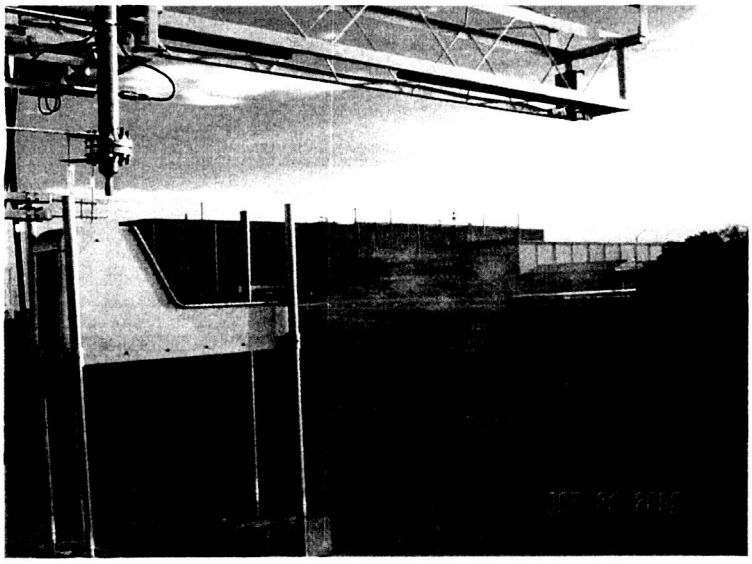

Figure 7b. Photograph of a jet flowing through a closed duct

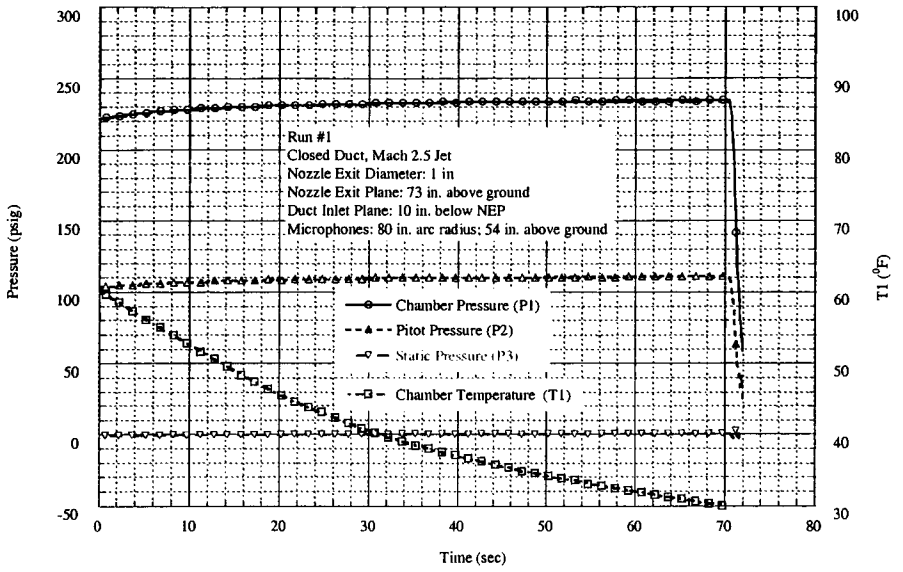

Figure 8a. Pressure and temperature history for Run 1 (closed duct)

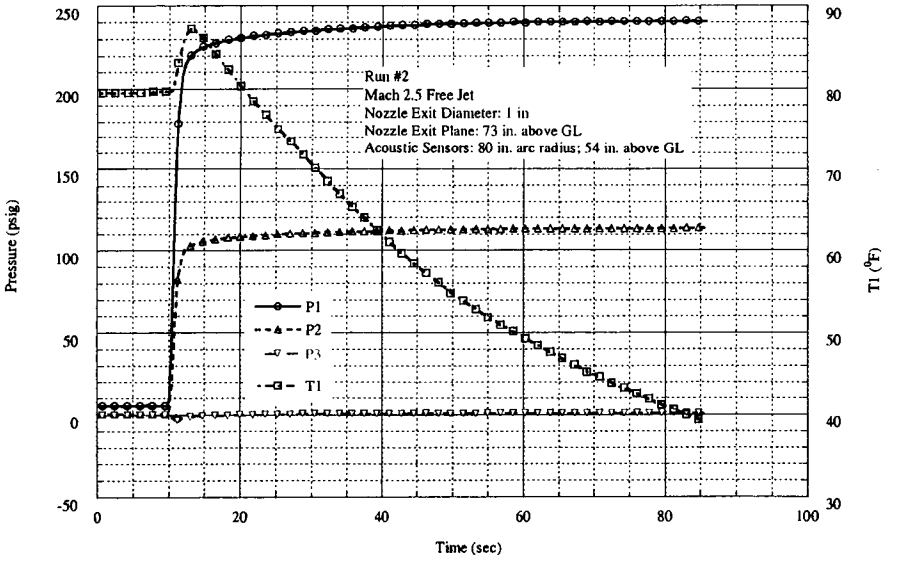

Figure 8b. Pressure and temperature history for Run 2 (free jet)

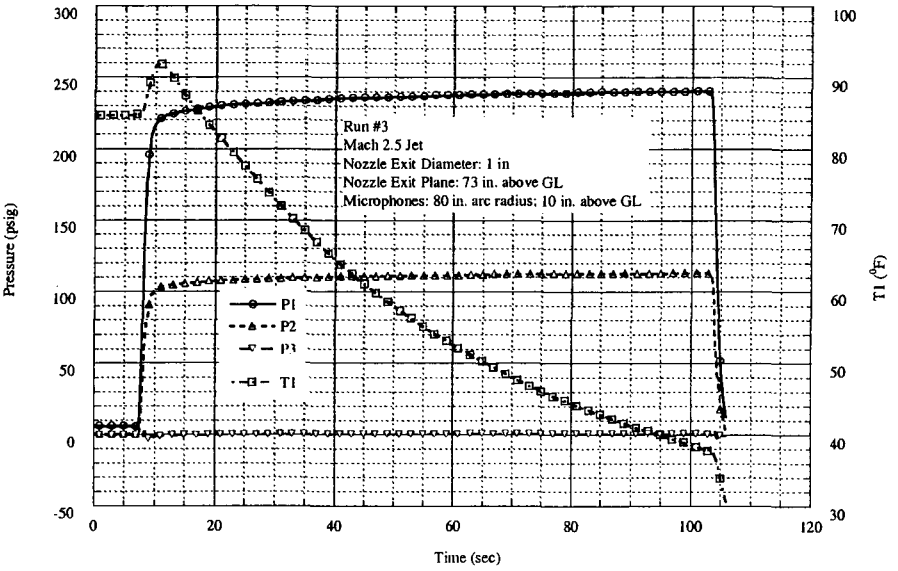

Figure 8c. Pressure and temperature history for Run 3 (free jet).

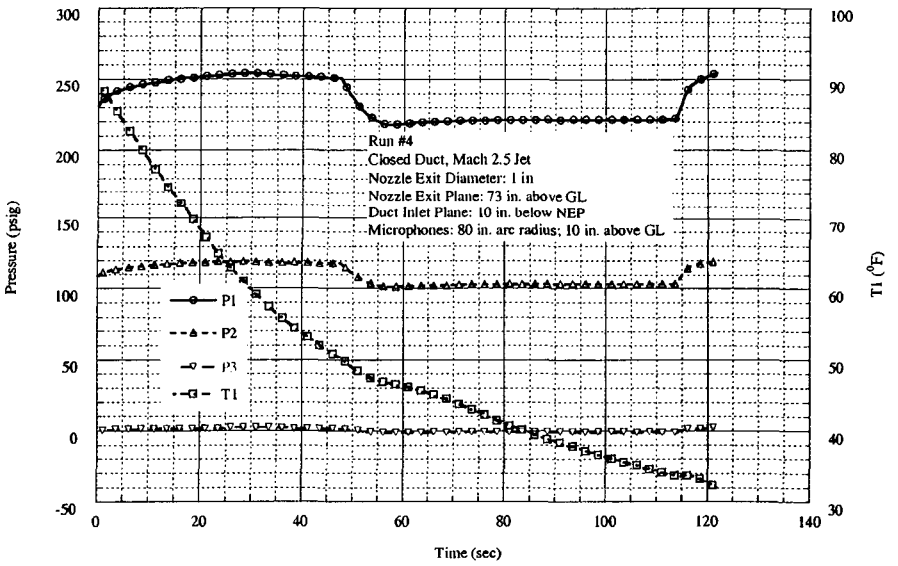

Figure 8d. Pressure and temperature history for Run 4 (closed duct)

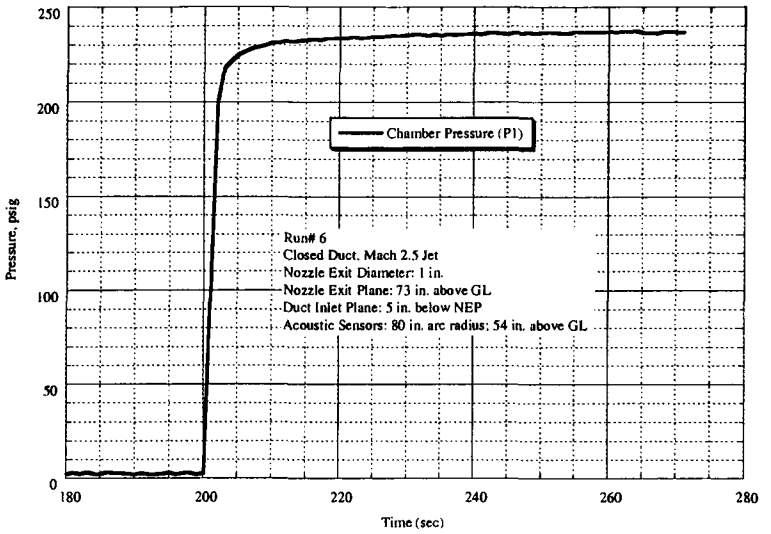

Figure 8e. Pressure and temperature history for Run 6 (closed duct)

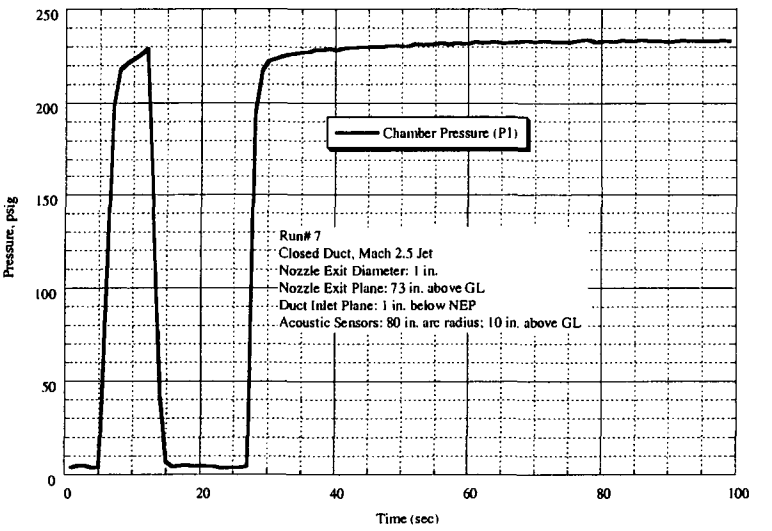

Figure 8f. Pressure and temperature history for Run 7 (closed duct)

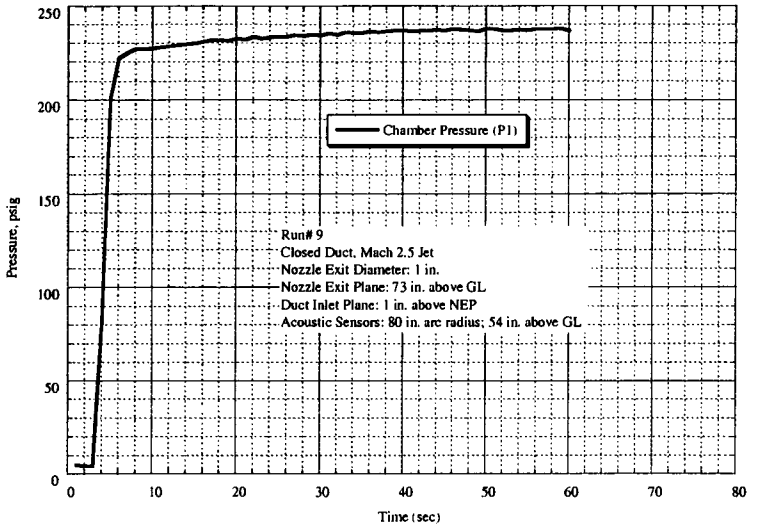

Figure 8g. Pressure and temperature history for Run 9 (closed duct)

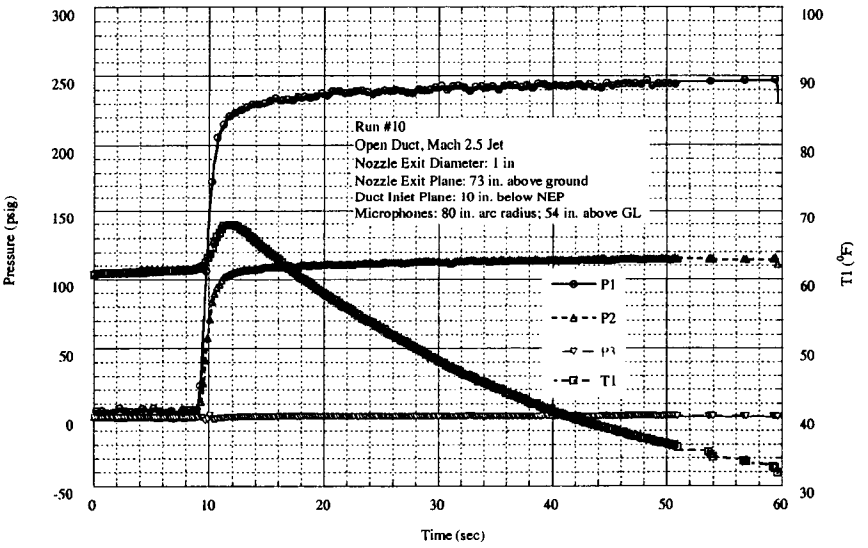

Figure 8h. Pressure and temperature history for Run 10 (open duct)

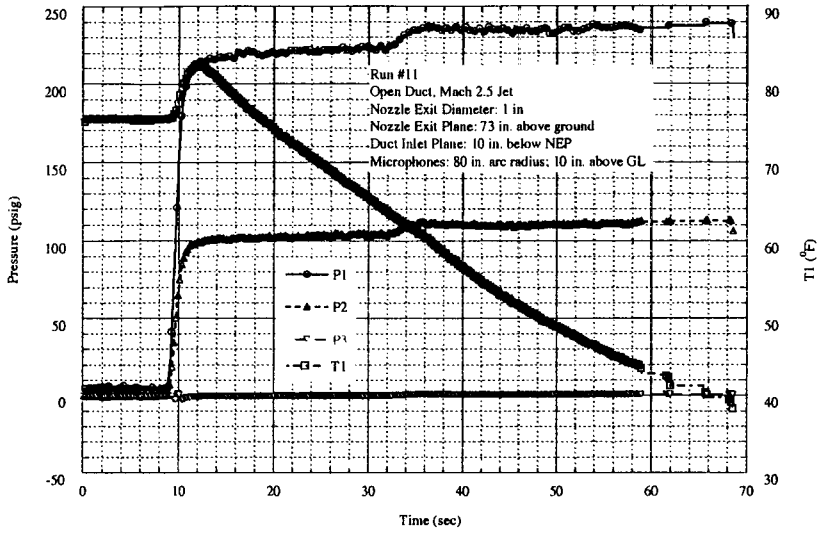

Figure 8i. Pressure and temperature history for Run 11 (open duct)

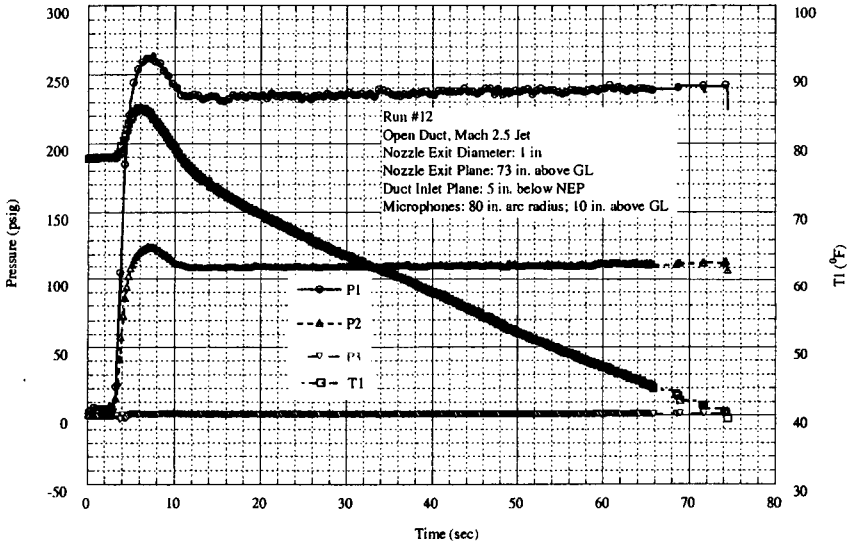

Figure 8j. Pressure and temperature history for Run 12 (open duct)

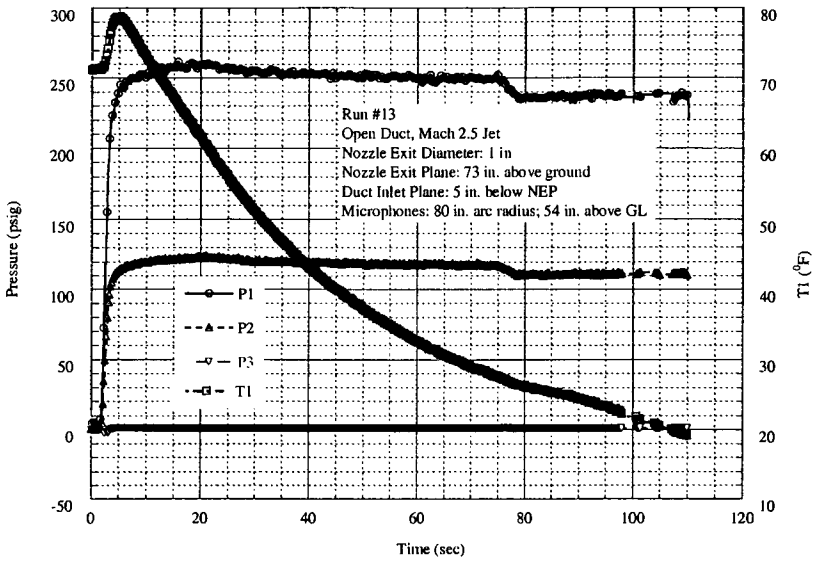

Figure 8k. Pressure and temperature history for Run 13 (open duct)

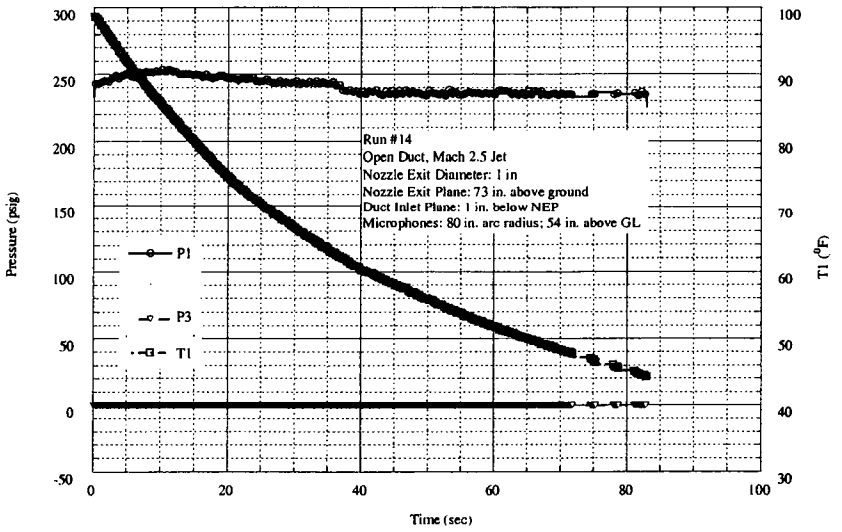

Figure 8l. Pressure and temperature history for Run 14 (open duct)

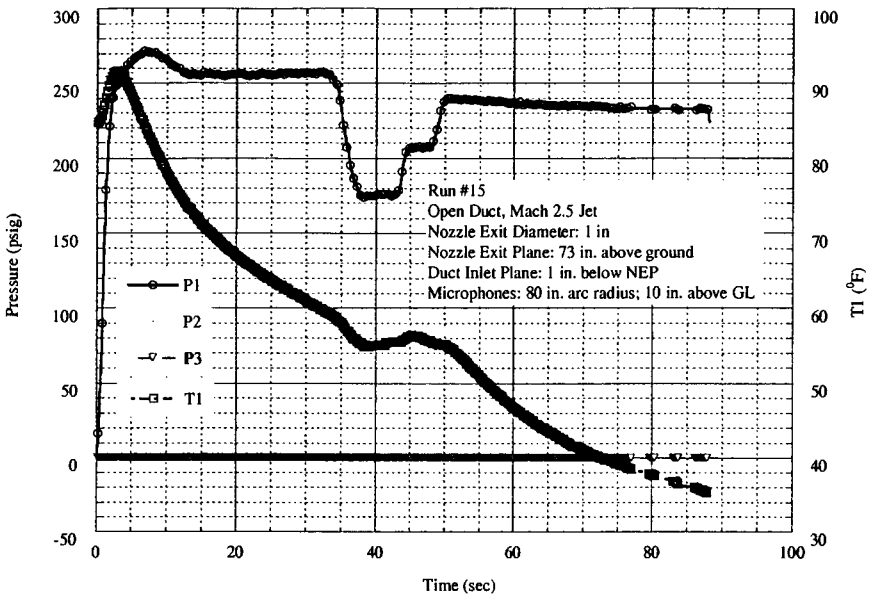

Figure 8m. Pressure and temperature history for Run 15 (open duct)

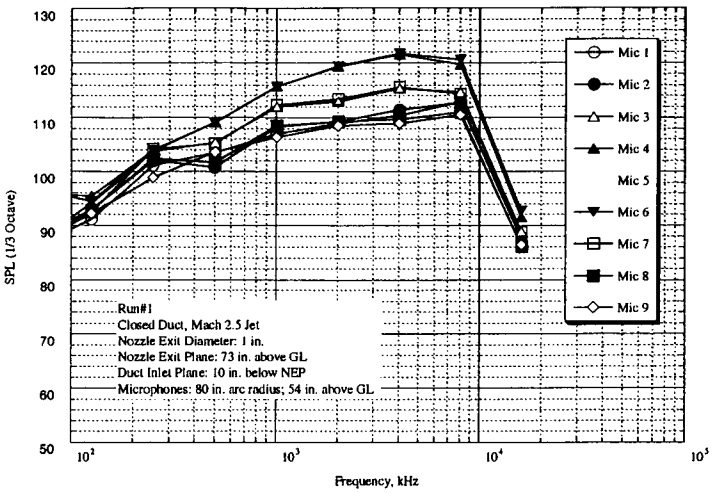

Figure 9a. Spectral sound power for Run 1 (closed duct)

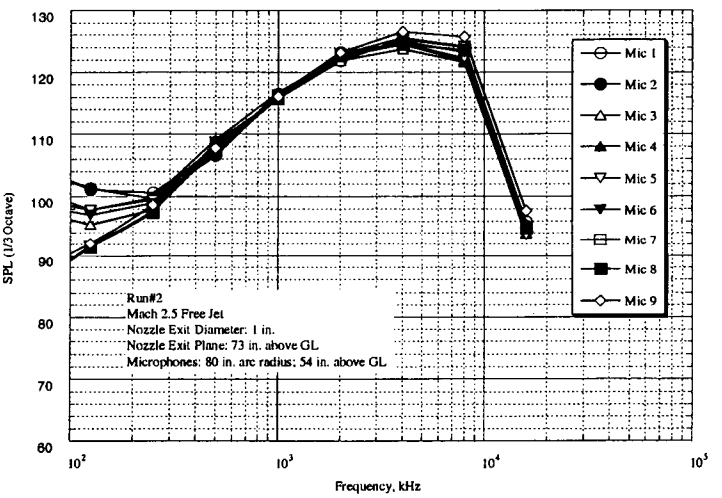

Figure 9b. Spectral sound power for Run 2 (free jet)

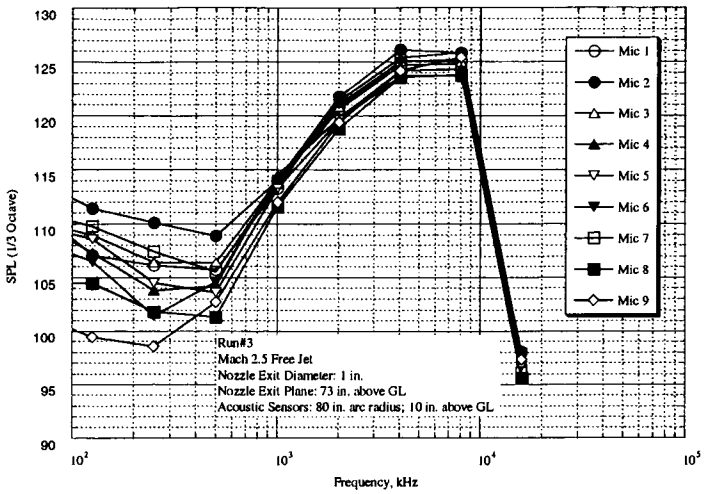

Figure 9c. Spectral sound power for Run 3 (free jet)

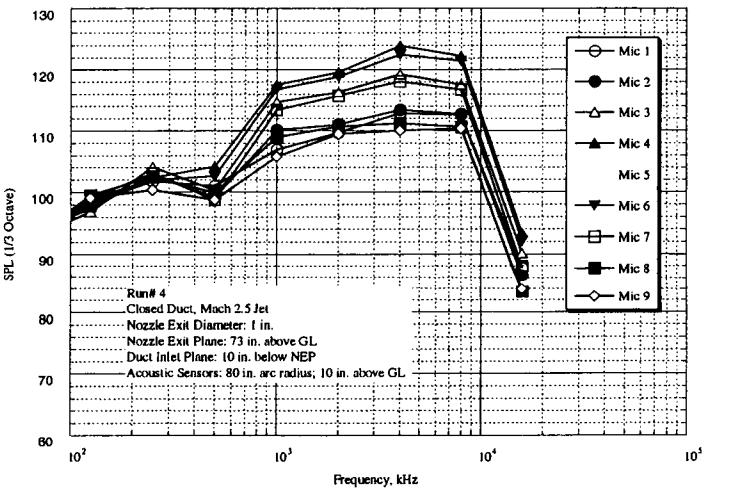

Figure 9d. Spectral sound power for Run 4 (closed duct)

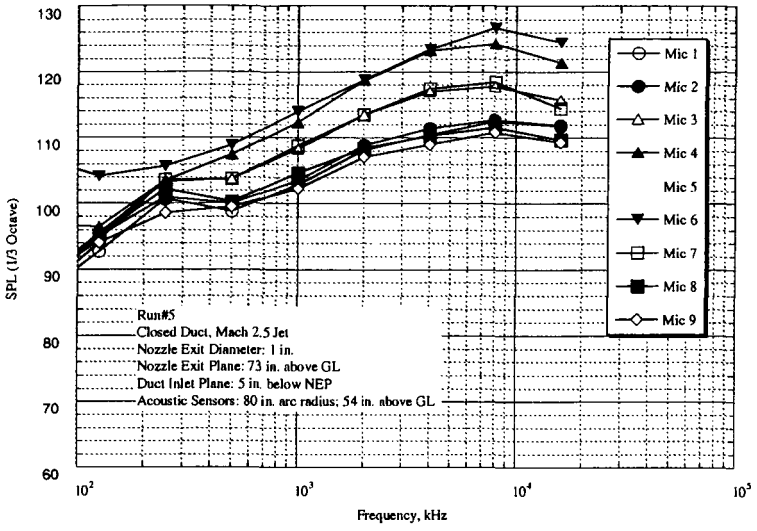

Figure 9e. Spectral sound power for Run 5 (closed duct)

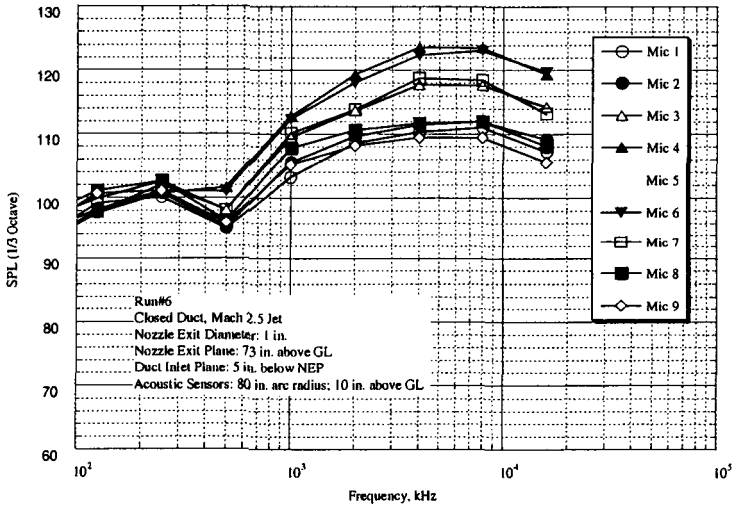

Figure 9f. Spectral sound power for Run 6 (closed duct)

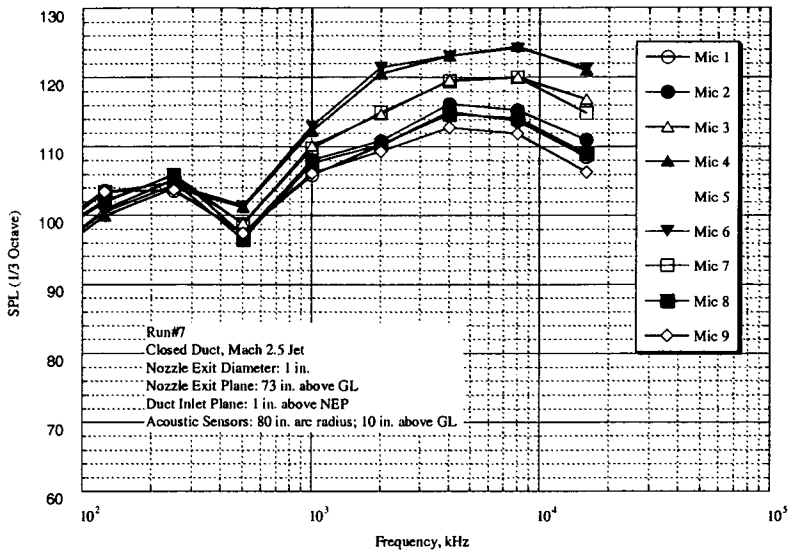

Figure 9g. Spectral sound power for Run 7 (closed duct)

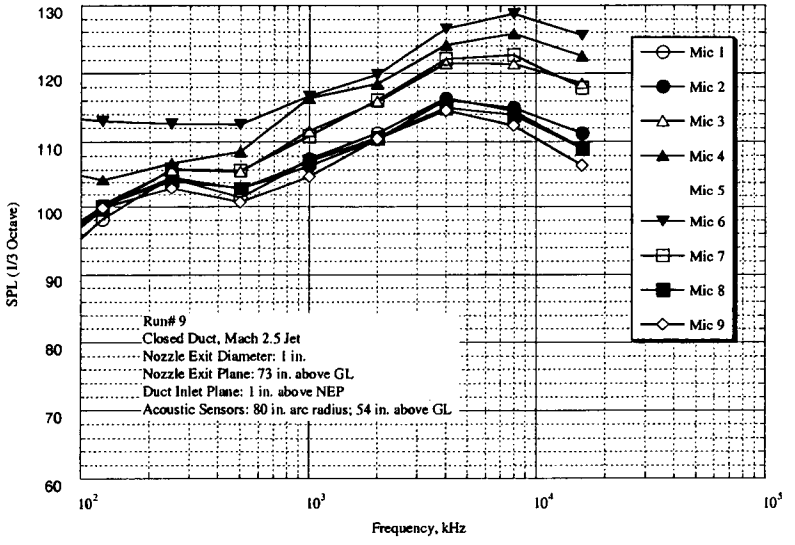

Figure 9h. Spectral sound power for Run 9 (closed duct)

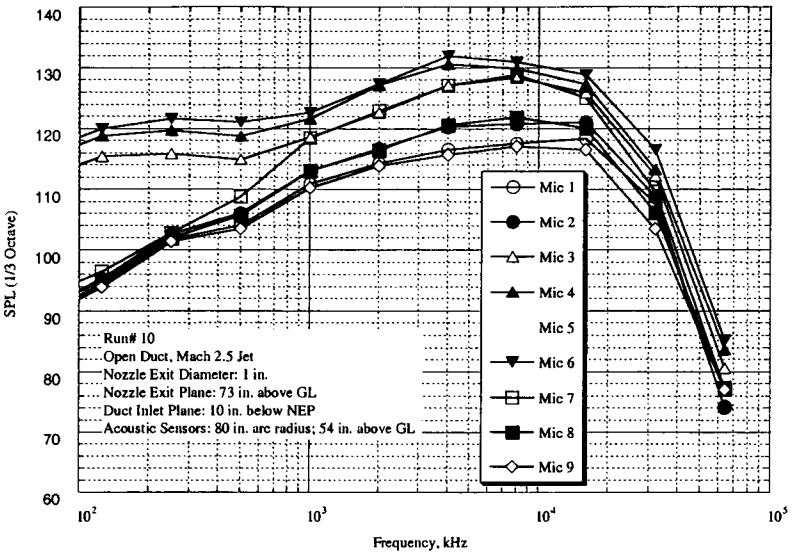

Figure 9i. Spectral sound power for Run 10 (open duct)

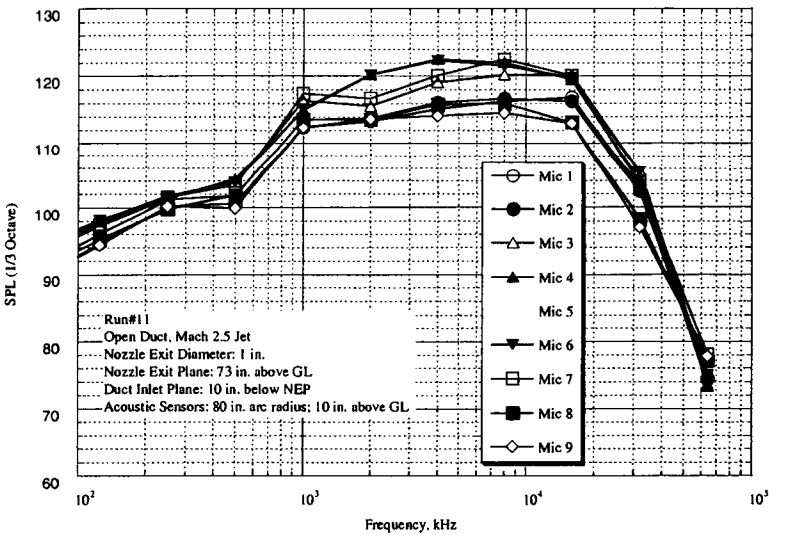

Figure 9j. Spectral sound power for Run 11 (open duct)

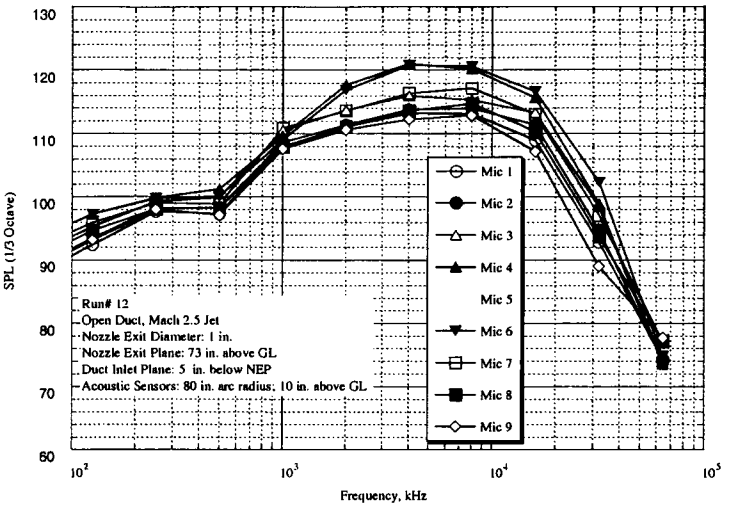

Figure 9k. Spectral sound power for Run 12 (open duct)

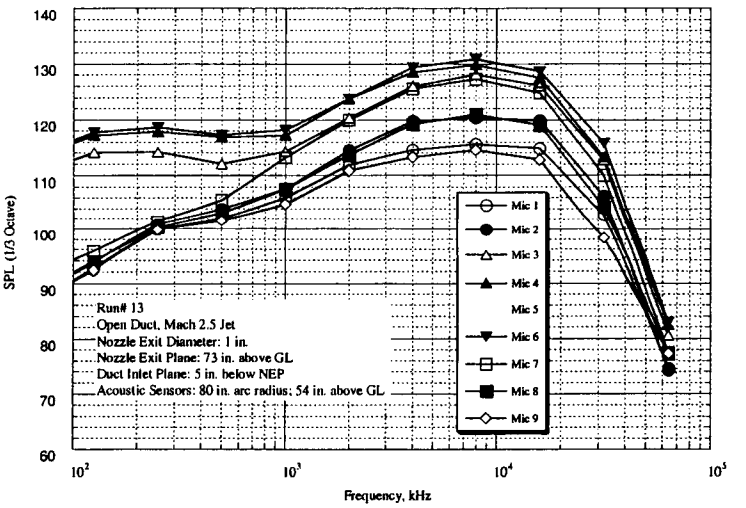

Figure 9l. Spectral sound power for Run 13 (open duct)

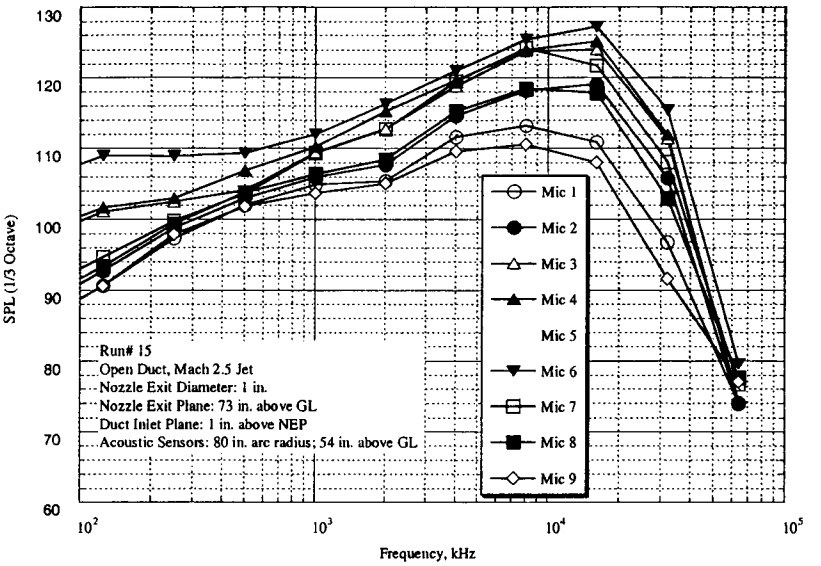

Figure 9m. Spectral sound power for Run 14 (open duct)

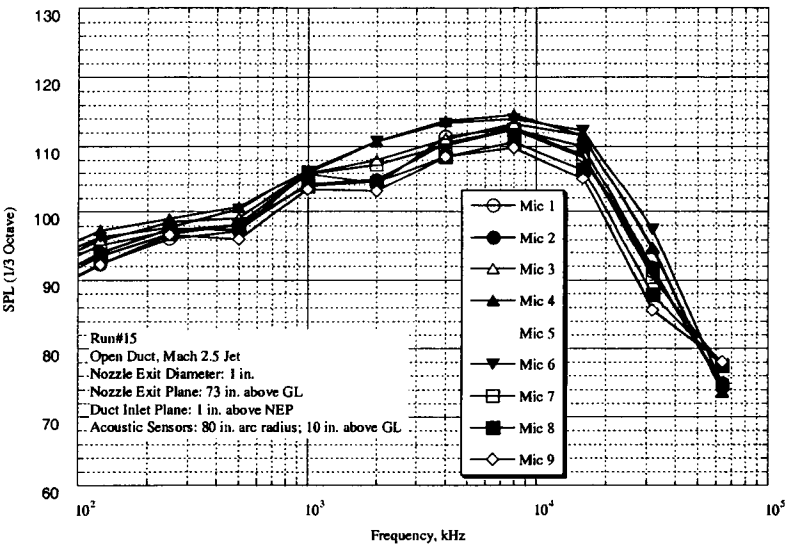

Figure 9n. Spectral sound power for Run 15 (open duct)

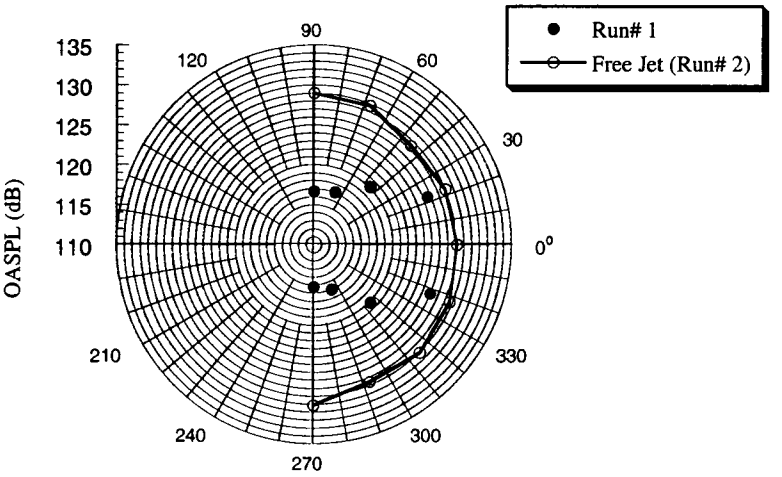

Run# 1
Closed Duct, Mach 2.5 Jet
Nozzle Exit Diameter: 1 in.
Nozzle Exit Plane: 73 in. above GL
Duct Inlet Plane: 10 in. below NEP
Acoustic Sensors: 80 in. arc radius; 54 in. above GL

Figure 10a. Directivity of OASPL for Run 1 (closed duct)

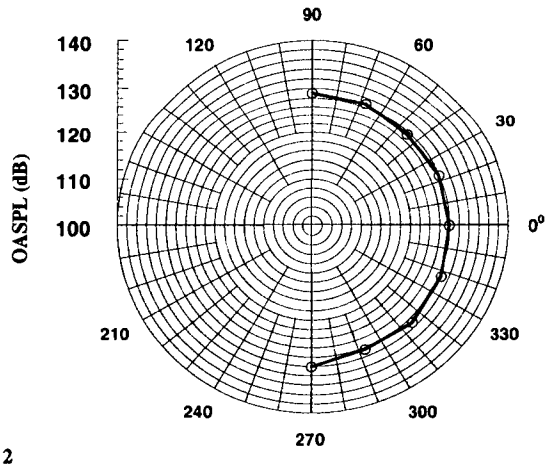

Run # 2
Mach 2.5 Free Jet
Nozzle Exit Diameter: 1 in.
Nozzle Exit Plane: 73 in. above GL
Acoustic Sensors: 80 in. arc radius; 54 in. above GL

Figure 10b. Directivity of OASPL for Run 2 (free jet)

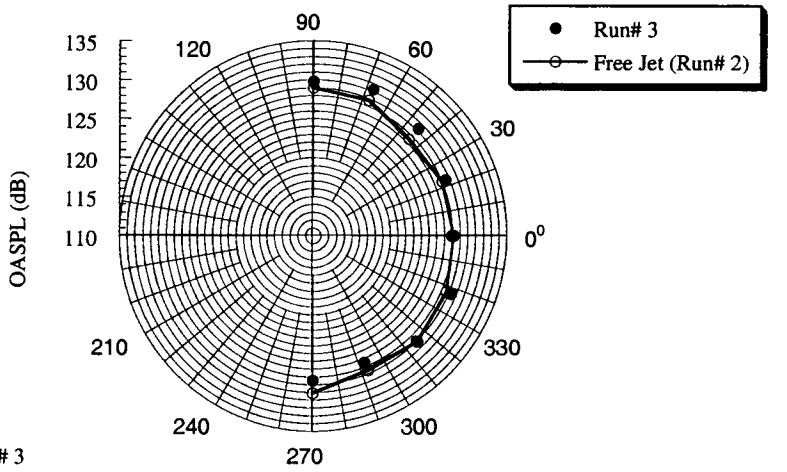

Run# 3
Mach 2.5, Free Jet
Nozzle Exit Diameter: 1 in.
Nozzle Exit Plane: 73 in. above GL
Acoustic Sensors: 80 in. arc radius; 10 in. above GL

Figure 10c. Directivity of OASPL for Run 3 (free jet)

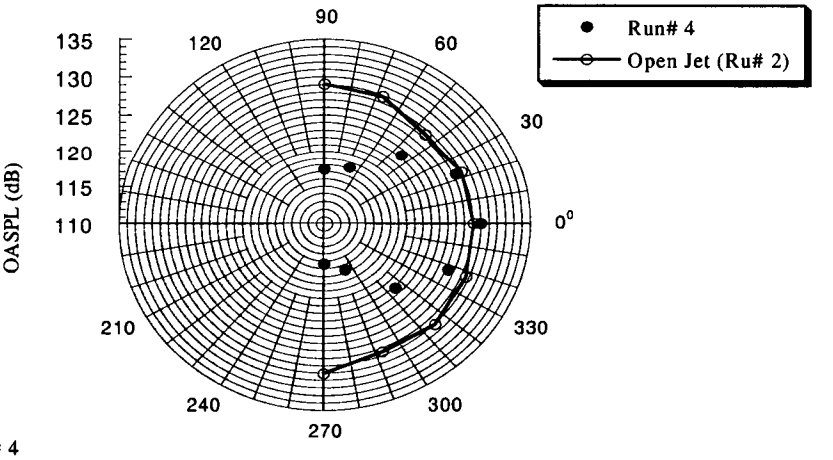

Run# 4
Closed Duct, Mach 2.5 Jet
Nozzle Exit Diameter: 1 in.
Nozzle Exit Plane: 73 in. above GL
Duct Inlet Plane: 10 in. below NEP
Acoustic Sensors: 80 in. arc radius; 10 in. above GL

Figure 10d. Directivity of OASPL for Run 4 (closed duct)

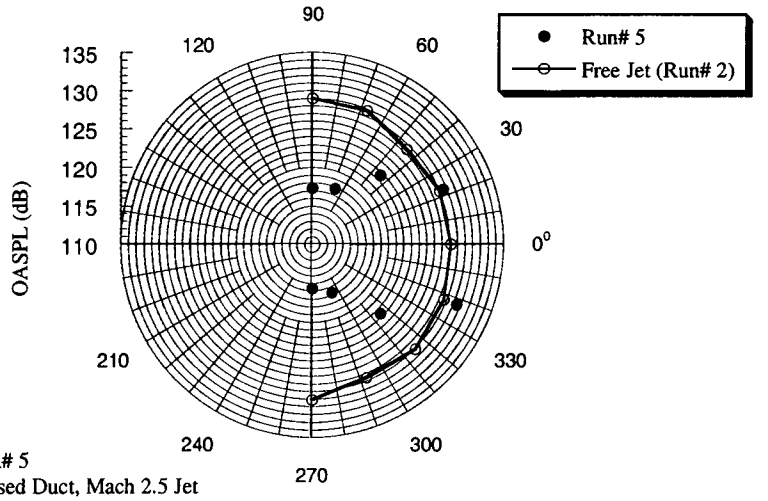

Run# 5
Closed Duct, Mach 2.5 Jet
Nozzle Exit Diameter: 1 in.
Nozzle Exit Plane: 73 in. above GL
Duct Inlet Plane: 5 in. below NEP
Acoustic Sensors: 80 in. arc radius; 54 in. above GL

Figure 10e. Directivity of OASPL for Run 5 (closed duct)

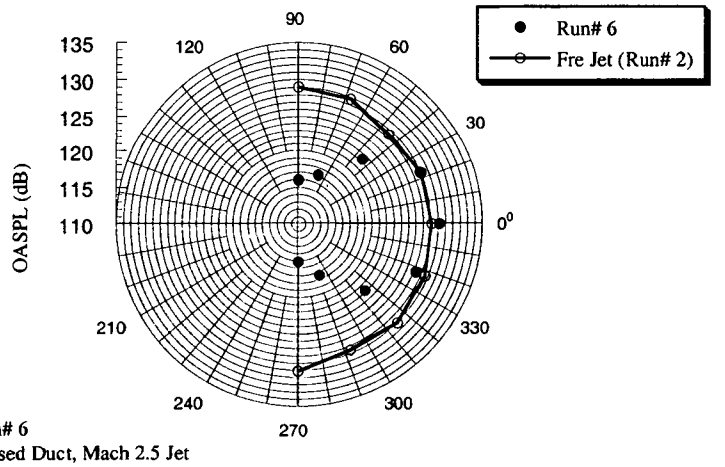

Run# 6
Closed Duct, Mach 2.5 Jet
Nozzle Exit Diameter: 1 in.
Nozzle Exit Plane: 73 in. above GL
Duct Inlet Plane: 5 in. below NEP
Acoustic Sensors: 80 in. arc radius; 10 in. above GL

Figure 10f. Directivity of OASPL for Run 6 (closed duct)

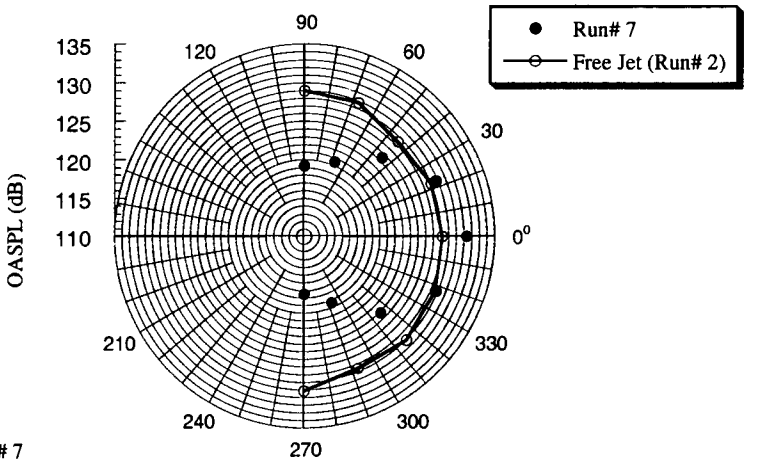

Run# 7
Closed Duct, Mach 2.5 Jet
Nozzle Exit Diameter: 1 in.
Nozzle Exit Plane: 73 in. above GL
Duct Inlet Plane: 1 in. above NEP
Acoustic Sensors: 80 in. arc radius; 10 in. above GL

Figure 10g. Directivity of OASPL for Run 7 (closed duct)

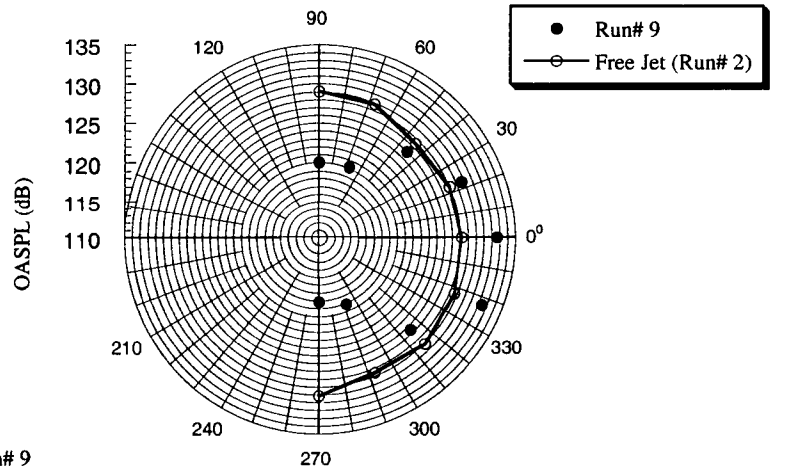

Run# 9
Closed Duct, Mach 2.5 Jet
Nozzle Exit Diameter: 1 in.
Nozzle Exit Plane: 73 in. above GL
Duct Inlet Plane: 1 in. above NEP
Acoustic Sensors: 80 in. arc radius; 54 in. above GL

Figure 10h. Directivity of OASPL for Run 9 (closed duct)

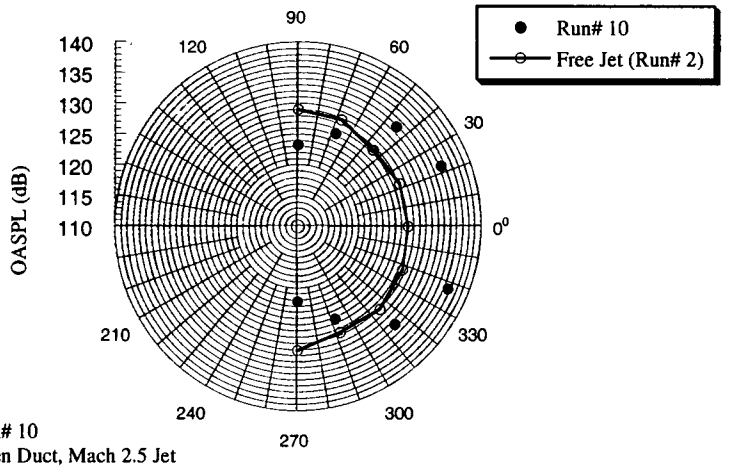

Run# 10
Open Duct, Mach 2.5 Jet
Nozzle Exit Diameter: 1 in.
Nozzle Exit Plane: 73 in. above GL
Duct Inlet Plane: 10 in. below NEP
Acoustic Sensors: 80 in. arc radius; 54 in. above GL

Figure 10i. Directivity of OASPL for Run 10 (open duct)

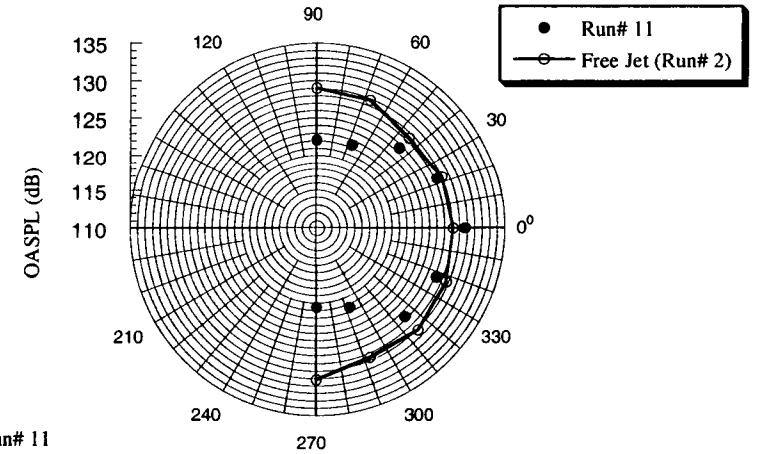

Run# 11
Open Duct, Mach 2.5 Jet
Nozzle Exit Diameter: 1 in.
Nozzle Exit Plane: 73 in. above GL
Duct Inlet Plane: 10 in. below NEP
Acoustic Sensors: 80 in. arc radius; 10 in. above GL

Figure 10j. Directivity of OASPL for Run 11 (open duct)

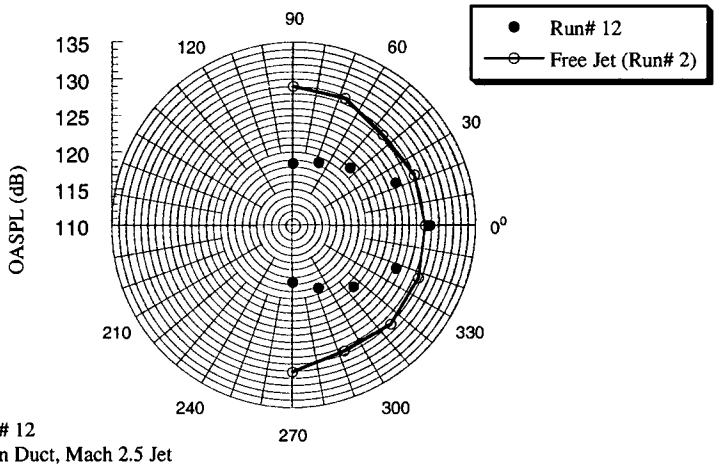

Run# 12
Open Duct, Mach 2.5 Jet
Nozzle Exit Diameter: 1 in.
Nozzle Exit Plane: 73 in. above GL
Duct Inlet Plane: 5 in. below NEP
Acoustic Sensors: 80 in. arc radius; 10 in. above GL

Figure 10k. Directivity of OASPL for Run 12 (open duct)

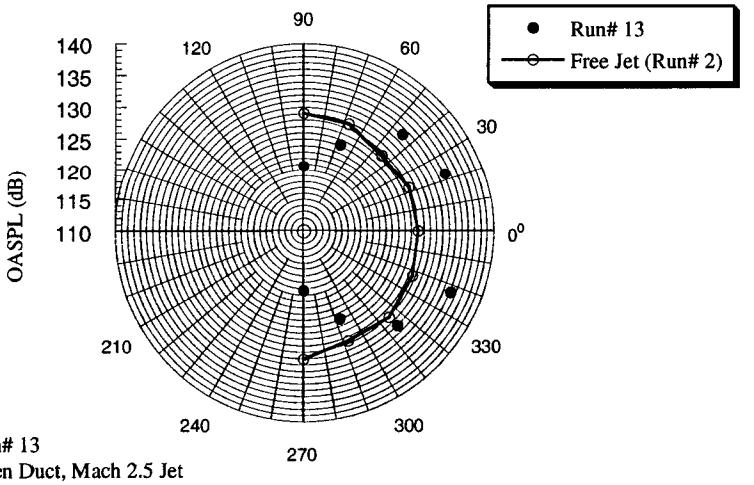

Run# 13
Open Duct, Mach 2.5 Jet
Nozzle Exit Diameter: 1 in.
Nozzle Exit Plane: 73 in. above GL
Duct Inlet Plane: 5 in. below NEP
Acoustic Sensors: 80 in. arc radius; 54 in. above GL

Figure 10l. Directivity of OASPL for Run 13 (open duct)

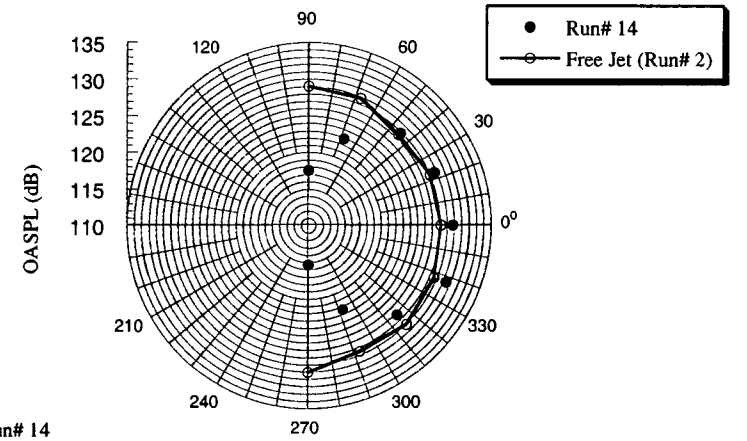

Run# 14
Open Duct, Mach 2.5 Jet
Nozzle Exit Diameter: 1 in.
Nozzle Exit Plane: 73 in. above GL
Duct Inlet Plane: 1 in. above NEP
Acoustic Sensors: 80 in. arc radius; 54 in. above GL

Figure 10m. Directivity of OASPL for Run 14 (open duct)

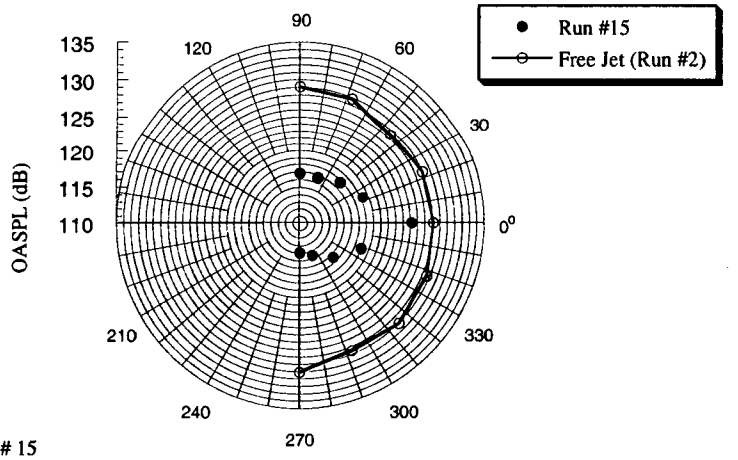

Run# 15
Open Duct, Mach 2.5 Jet
Nozzle Exit Diameter: 1 in.
Nozzle Exit Plane: 73 in. above GL
Duct Inlet Plane: 1 in. below NEP
Acoustic Sensors: 80 in. arc radius; 10 in. above GL

Figure 10n. Directivity of OASPL for Run 15 (open duct)

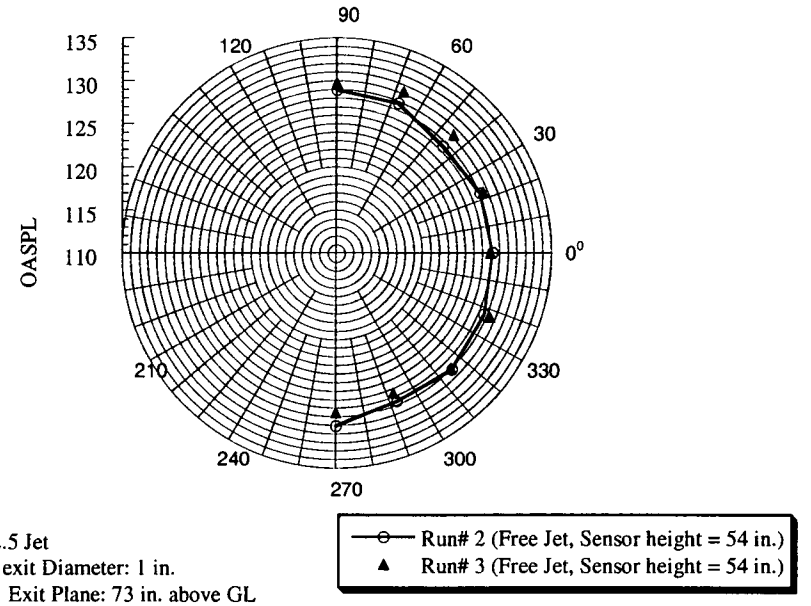

Figure 11a. Ground effect on OASPL for a free jet with the NEP at 10 inches above the duct inlet plane

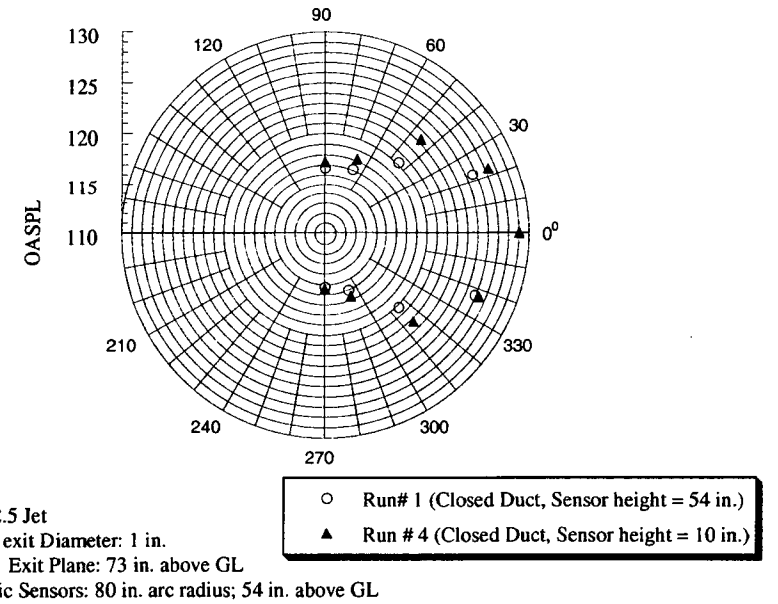

Figure 11b. Ground effect on OASPL for a closed duct with the NEP at 10 inches above the duct inlet plane

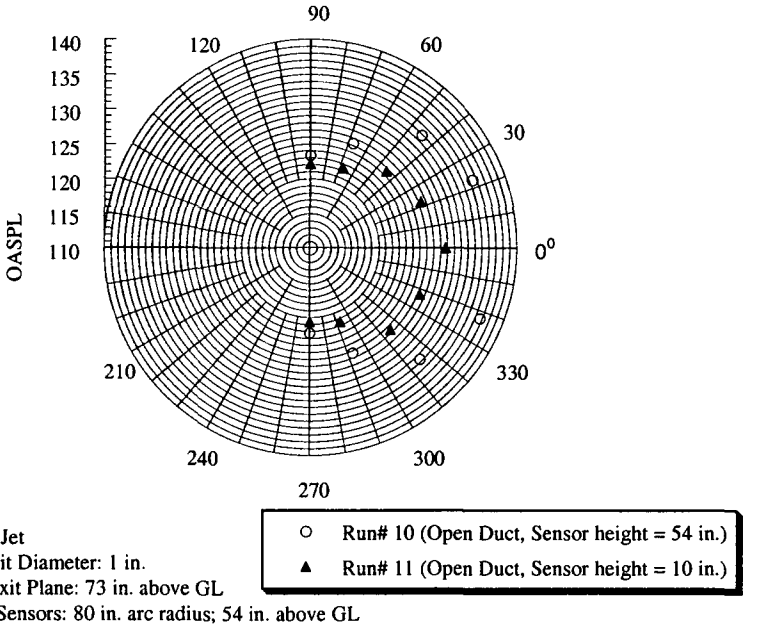

Figure 11c. Ground effect on OASPL for an open duct with the NEP at 10 inches above the duct inlet plane

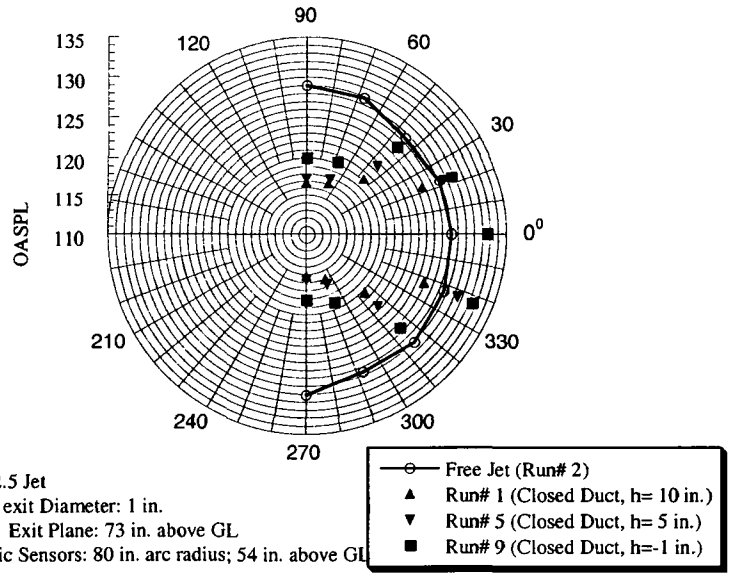

Figure 12a. Effect of nozzle exit plane height (relative to duct inlet plane) for a closed duct

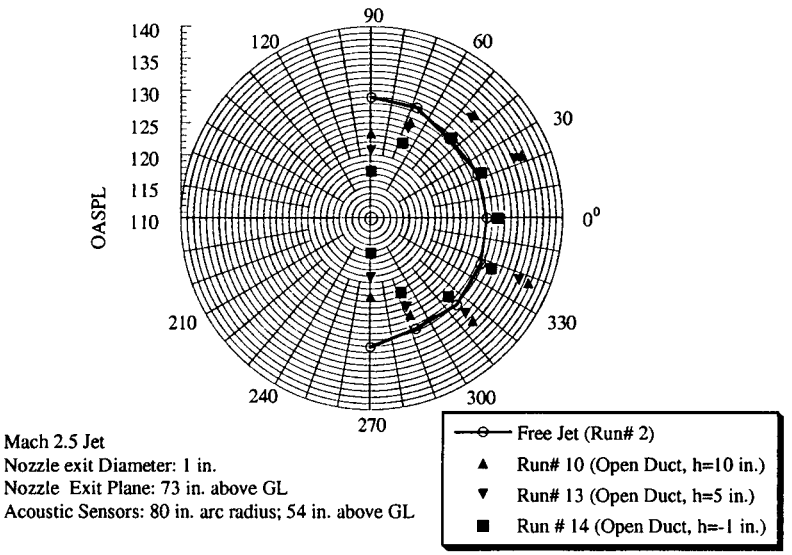

Figure 12b. Effect of nozzle exit plane height (relative to duct inlet plane) for an open duct

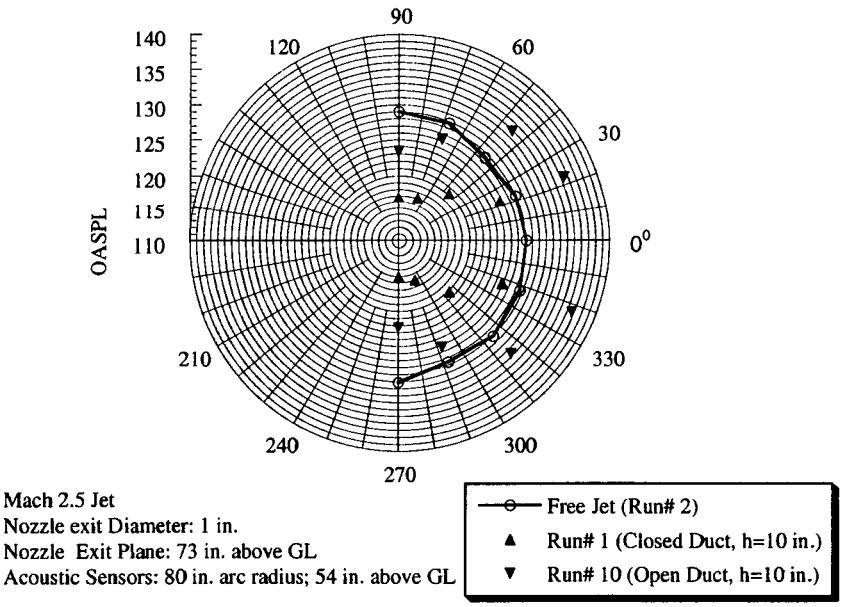

Figure 13a. Comparison of OASPL for a closed duct and an open duct with the NEP at 10 inches above the duct inlet plane

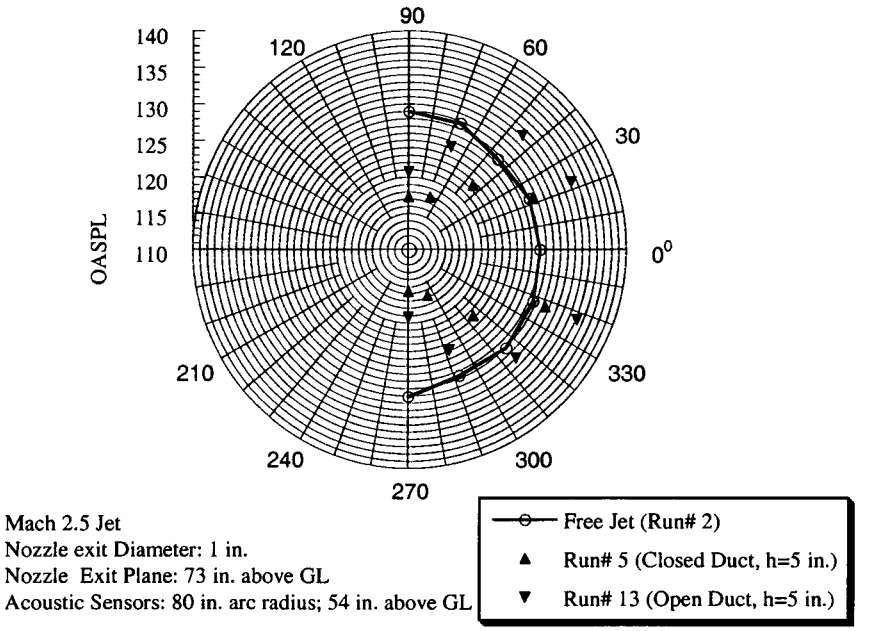

Figure 13b. Comparison of OASPL for a closed duct and an open duct with the NEP at 5 inches above the duct inlet plane

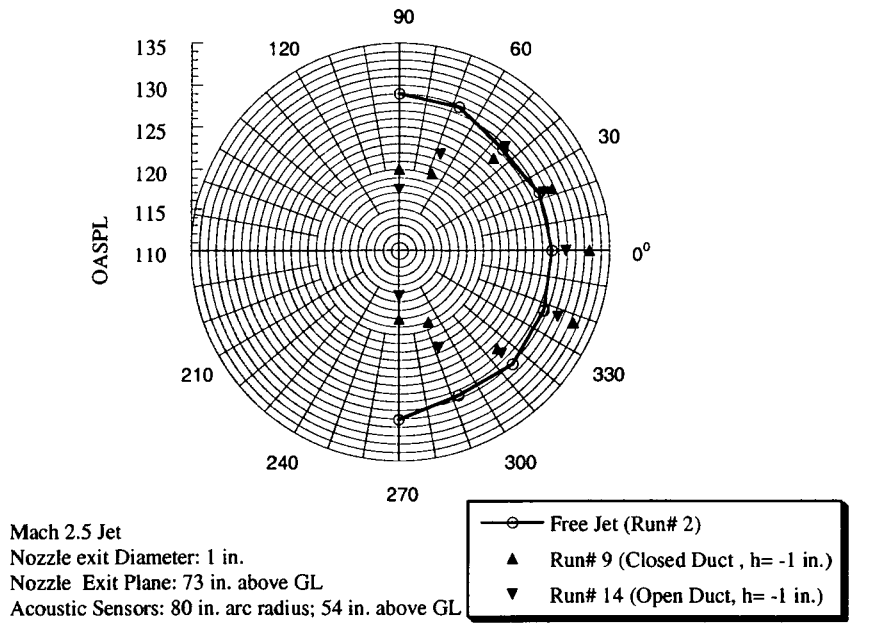

Figure 13c. Comparison of OASPL for a closed duct and an open duct with the NEP at 1 inch below the duct inlet plane

APPENDIX A

LabView Description

Appendix A gives the LabView details for calibration and data acquisition and analysis. As previously indicated, all the LabView effort is due to Geoffrey Rowe of Swales (USTDC).

A-1 CALIBRATION

Figures A-1a and A-1b show typical plots from LabView describing the calibration of a single microphone at 1000 Hz for SPL of 114 dB and 94 dB respectively. The plots display the pressure-time history, the spectral power density, and the sound pressure level spectrum.

A more automated result for the calibration of all the nine microphones at 114 dB (at 1 kHz) for Run 12 is exhibited in Figure A-2.

A-2 PRESSURE AND TEMPERATURE HISTORY

A raw plot of chamber pressure (P1), chamber temperature (T1), pitot pressure (P2) and static pressure (P3) is illustrated in Figure A-3.

A-3 MICROPHONE TIME TRACE

Figure A-4 shows a typical trace of the raw microphone pressure-time signal $p'(t)$ for Run 12, microphone 9. The corresponding power spectral density and SPL spectrum are also shown here.

A-4 SOUND PRESSURE LEVEL SPECTRUM AND OASPL

The SPL spectrum and the OAPSL of the microphones for Run 12 are sketched in Figure A-5. In the OAPSL plot, the result of the free jet, showing nearly a symmetric character, is also presented for comparison purposes.

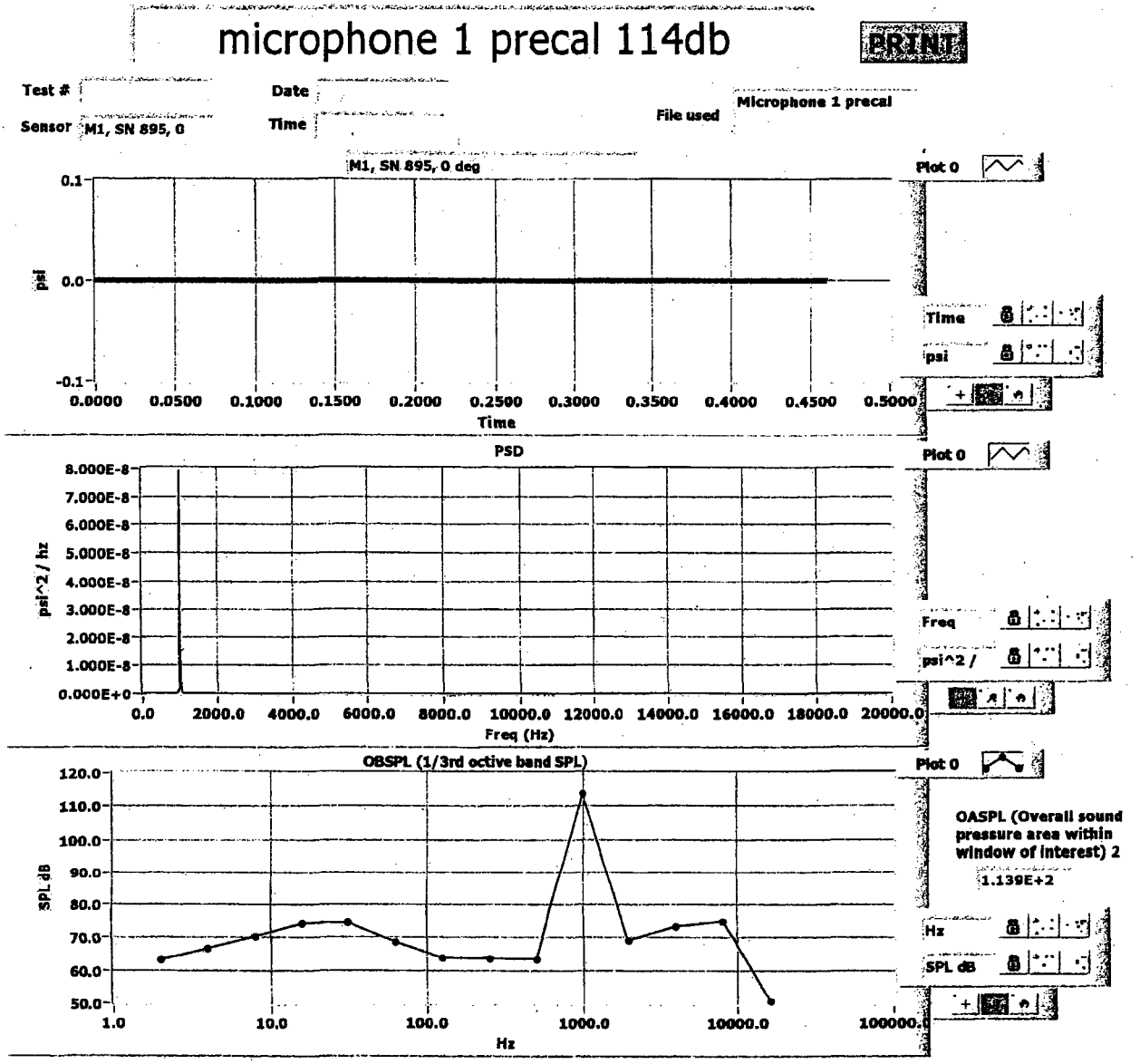

Figure A-1a. Calibration of single microphone at 1000 Hz for SPL of 114 dB

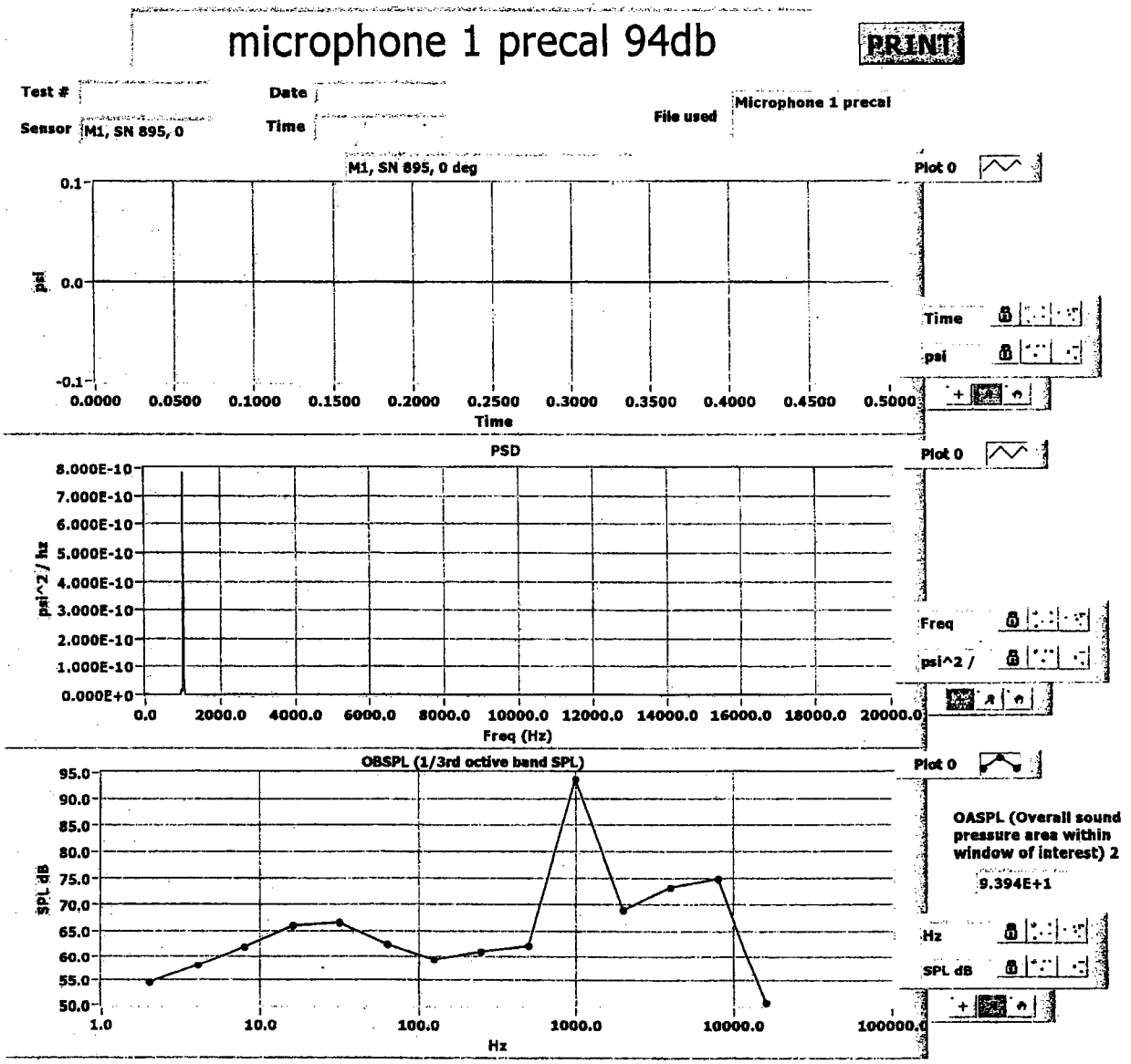

Figure A-1b. Calibration of single microphone at 1000 Hz for SPL of 94 dB

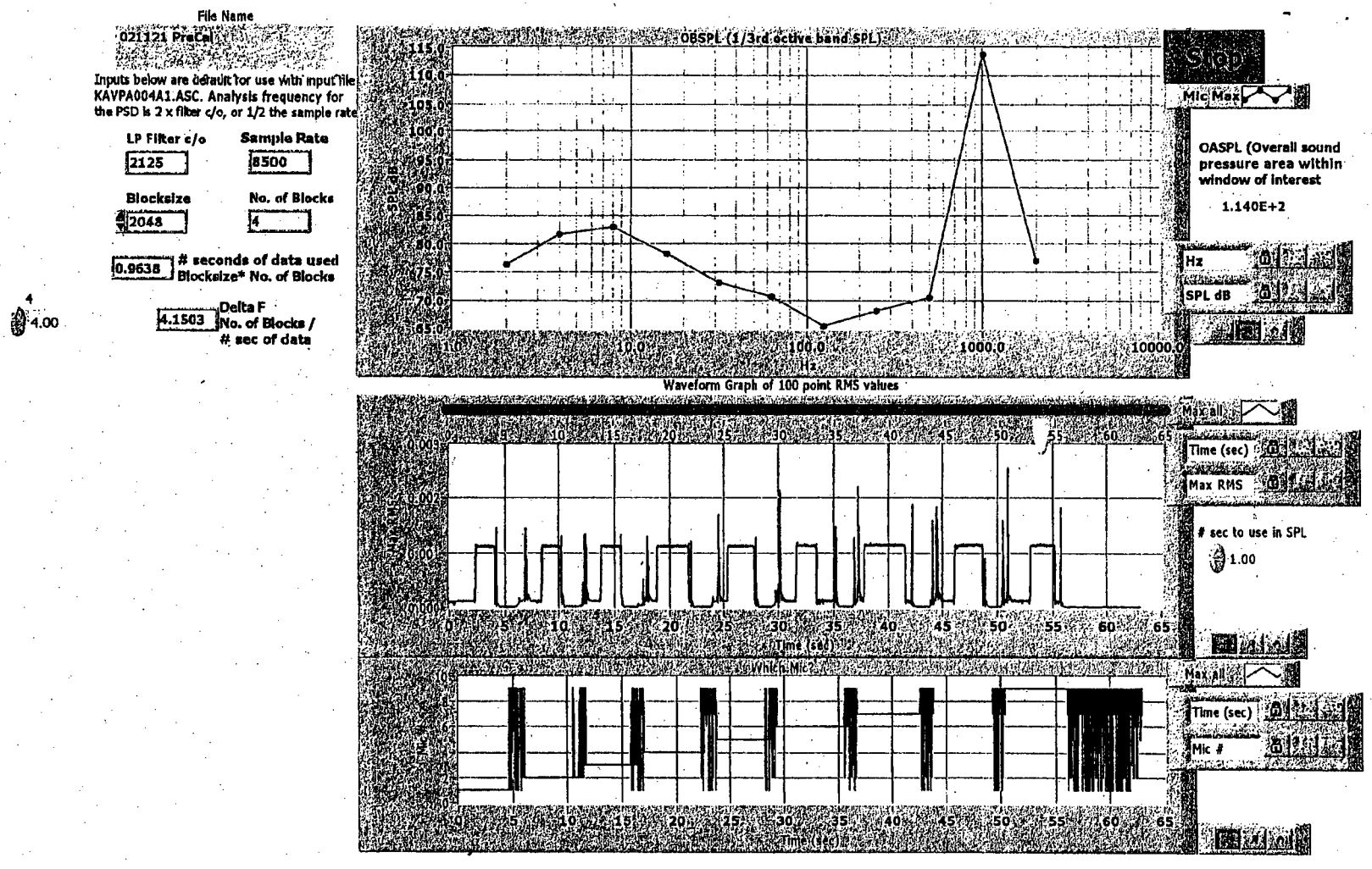

Figure A-2. Calibration of all microphones

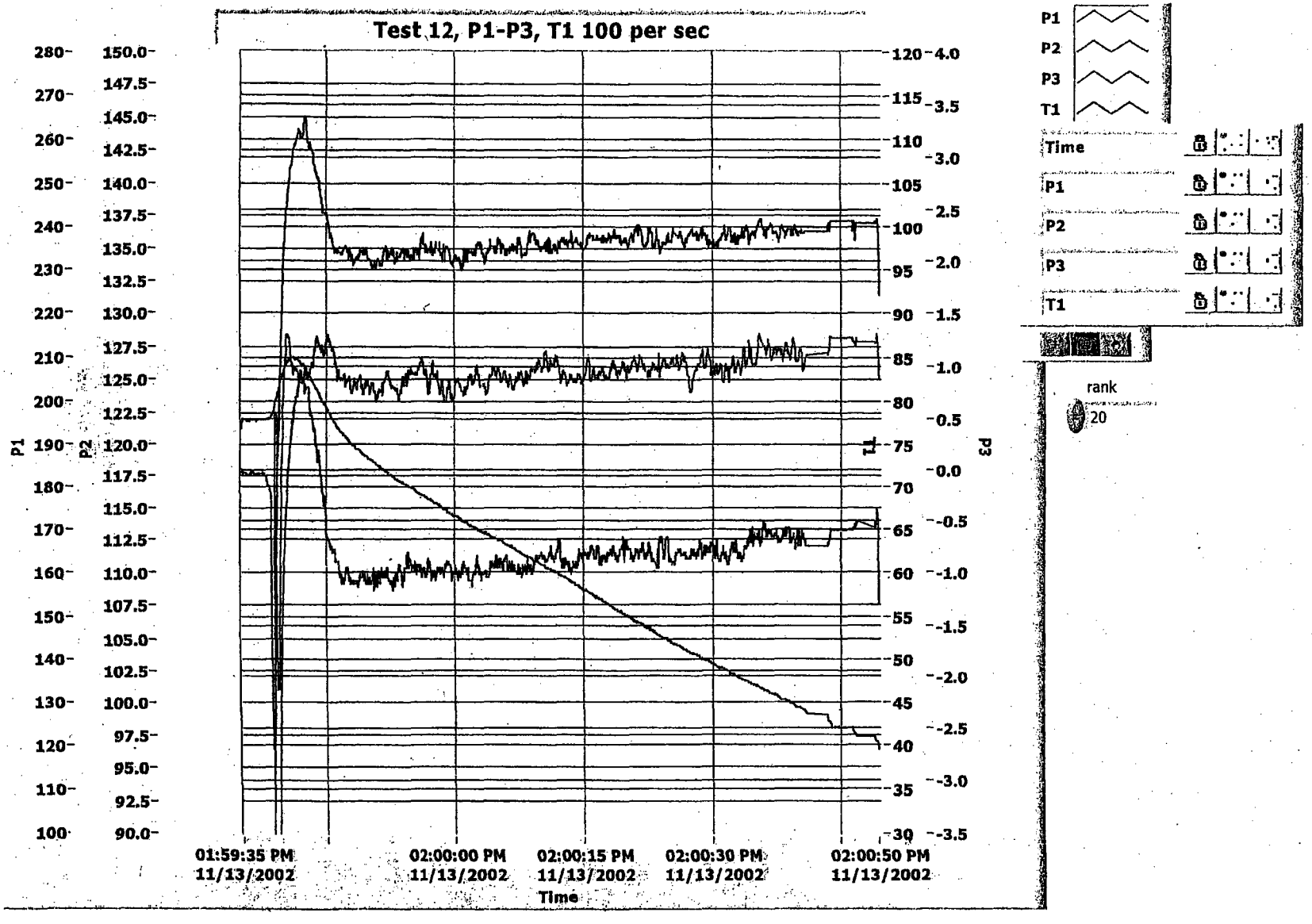

Figure A-3. Pressure and temperature history

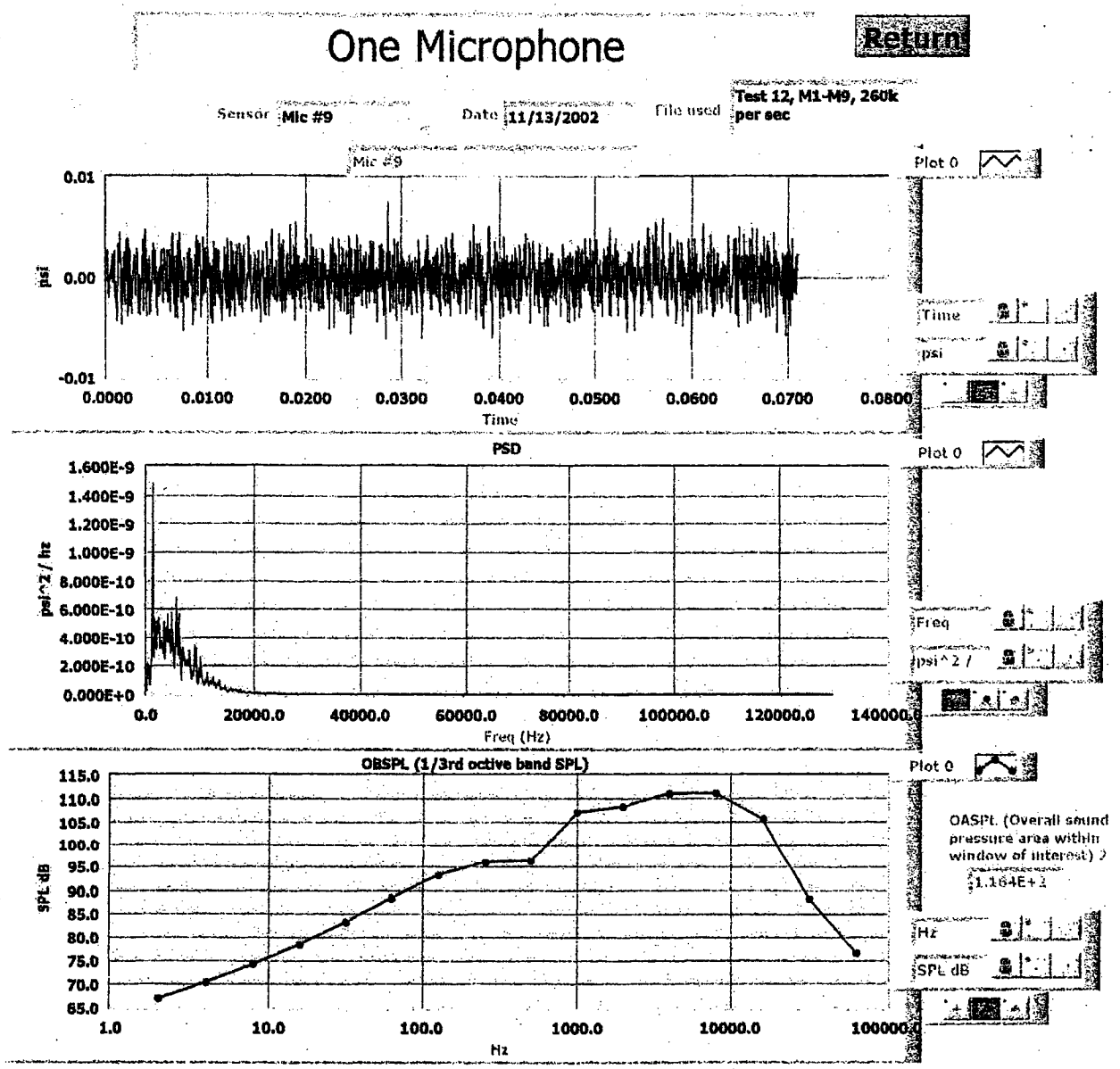

Figure A-4. Microphone pressure-time signal

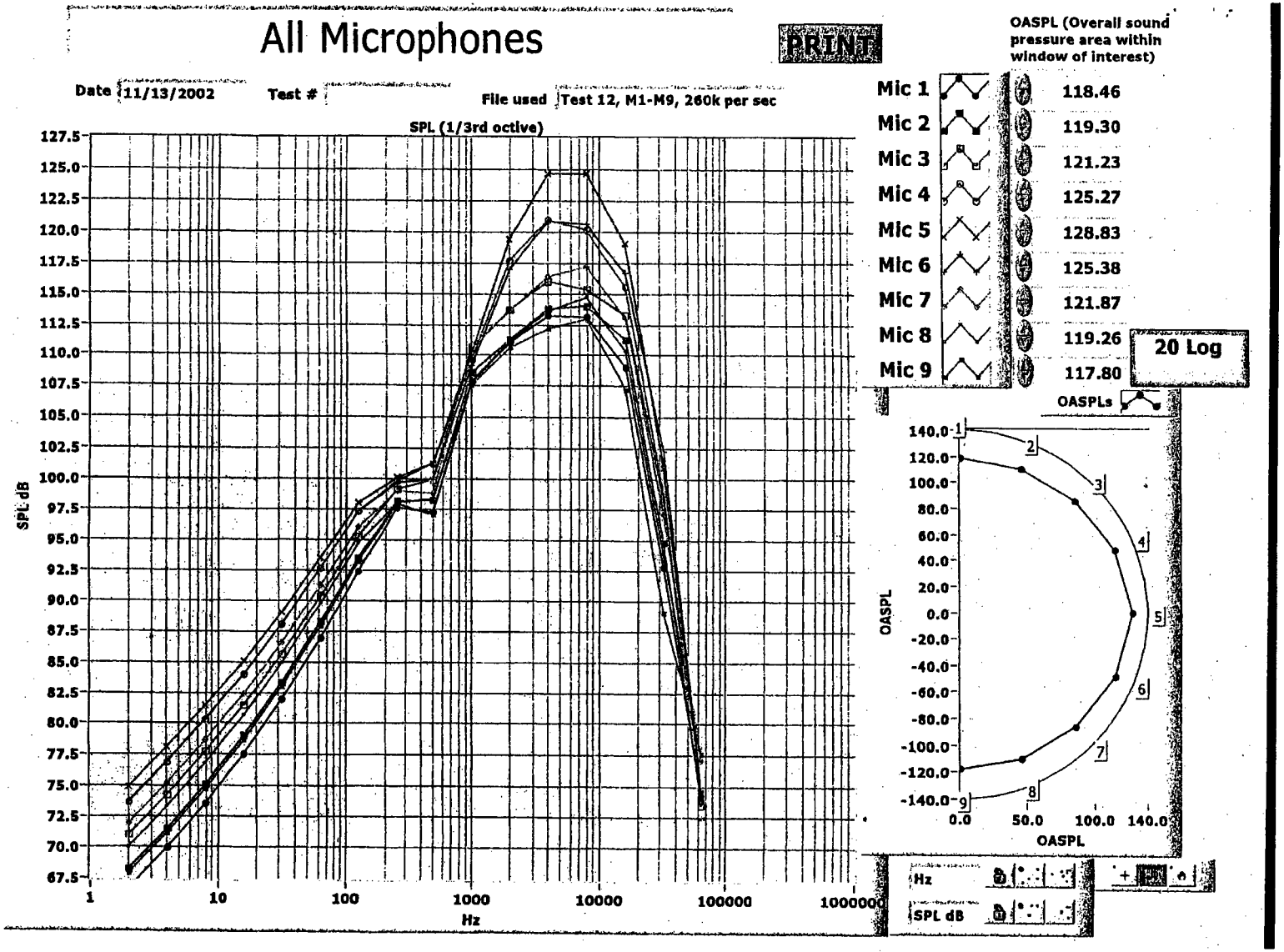

Figure A-5. SPL spectrum and OASPL of all microphones

REPORT DOCUMENTATION PAGE

Form Approved
OMB No. 0704-0188

1. AGENCY USE ONLY *(Leave blank)*	2. REPORT DATE	3. REPORT TYPE AND DATES COVERED
	April 2003	**NASA Technical Memorandum**

4. TITLE AND SUBTITLE
NASA/TM-2003-211186, Scale Model Experiments on Sound Propagation From a Mach 2.5 Cold Nitrogen Jet Flowing Through a Rigid-Walled Duct With a J-Deflector

5. FUNDING NUMBERS

6. AUTHOR(S)
Max Kandula, Sierra Lobo, Inc. (USTDC), and Bruce Vu, YA-C2-T

7. PERFORMING ORGANIZATION NAME(S) AND ADDRESS(ES)
John F. Kennedy Space Center
Kennedy Space Center, FL 32899

8. PERFORMING ORGANIZATION REPORT NUMBER

9. SPONSORING/MONITORING AGENCY NAME(S) AND ADDRESS(ES)
National Aeronautics and Space Administration
Washington, DC 20546-0001

10. SPONSORING/MONITORING AGENCY REPORT NUMBER
NASA/TM-2003-211186

11. SUPPLEMENTARY NOTES

12a. DISTRIBUTION/AVAILABILITY STATEMENT
Unclassified - Unlimited
Distribution: Standard
Availability: NASA CASI

12b. DISTRIBUTION CODE

13. ABSTRACT *(Maximum 200 words)*

This report summarizes the cold jet acoustic testing for Mach 2.5 supersonic nitrogen jet issuing from a nozzle with 1-inch exit diameter. Acoustic data, including spectral sound power and Overall Sound Pressure Level (OASPL), are obtained both for a free jet and with the jet flowing through a rigid-walled duct with a J-deflector. The relative performance of closed duct and open duct is evaluated. The results show that the closed duct is superior to the partially open duct, and results in about 3-decibel (dB) noise reduction (near the duct axis) relative to the free jet. The location of the nozzle exit plane (NEP) relative to the duct inlet plane (DIP) has a significant effect on the acoustic field. The results suggest that the location of NEP at 10 inches above the DIP results in reduced acoustic loads relative to 5 inches above the duct inlet and 1 inch into the duct inlet.

14. SUBJECT TERMS
Sound propagation, J-deflector, cold jet acoustic testing

15. NUMBER OF PAGES
61

16. PRICE CODE

17. SECURITY CLASSIFICATION OF REPORT	18. SECURITY CLASSIFICATION OF THIS PAGE	19. SECURITY CLASSIFICATION OF ABSTRACT	20. LIMITATION OF ABSTRACT
unclassified	**unclassified**	**unclassified**	**unlimited**

NSN 7540-01-280-5500

Standard Form 298 Rev. 2-89)
Prescribed by ANSI Std. Z-39-18
298-102